journal

J. Am. Ceram. Soc., 81 [4] 815–36 (1998)

Technical Cost Framework for High-Temperature Manufacturing of Small Components and Devices

Anthony G. Evans,* John W. Hutchinson,* Robert G. Hutchinson, and Yuki Sugimura

Division of Engineering and Applied Sciences, Harvard University, Cambridge, Massachusetts 02138

Tian Jian Lu

Engineering Department, University of Cambridge, Cambridge CB2 1PZ, United Kingdom

The high-temperature step that is required in a manufacturing process can contribute substantially to the cost. A technical cost framework (TCF) that allows trends in these costs to be determined as a function of the essential variables provides opportunities for their minimization. The basic variables are the furnace capacity, the operating temperature, and the furnace construction. The dependent variables are power, acquisition, and replacement. Information from thermal and process models as well as the furnace element life expectancy provides the functions needed to conduct the minimization through the TCF. The overall strategy is developed and illustrated with examples.

I. Introduction

One goal of manufacturing process development is the discovery of a method for processing a material into components or devices that attain explicit property and performance specifications at *minimum cost.* These specifications usually are established by the system level design strategy. Establishing a methodology that links these aspects in a systematic manner is elusive. One approach that provides focus and may lead to a tractable methodology embraces a technical cost framework (TCF). This framework interrelates parameters from design and manufacturing through a structure that accepts output from both process simulations and design calculations. The approach is simple and direct. The challenge is to establish a modeling environment that either calculates or measures the input parameters with acceptable certainty. The concept is not informative in the abstract. Examples are needed to illustrate the approach and the potential for its further development. An illustration is presented for a product yet to achieve market penetration primarily because of cost considerations.

The TCF approach is most applicable when the manufacturing steps are clearly defined, albeit that several alternatives for making an acceptable product may exist. Then, iterations and optimizations that establish acceptable performance at lowest cost can be performed. Often one step dominates the cost because of either expensive capital acquisition or high power requirements, combined with long cycle times. Identifying this step and finding approaches for substantially reducing the associated costs are the essential issues.

When a high-temperature step is involved, it often dominates the nonmaterial contributions to the cost. There are many innovative means for addressing this cost challenge. In the present article, various methods commonly used for heat treatment are examined to facilitate a logical decision about the preferred approach in any new manufacturing initiative. The philosophy evolves around the expectation that the market for the products is substantial enough to allow the furnace to operate at *maximum capacity,* with allowance for downtime required for maintenance and repair. Then, the cost consequences of operating below capacity can be systematically addressed. The mix of product geometries and properties that govern application are considered to be sufficiently similar that property development occurs in essentially the same way for all products, such that *yields can be controlled and characterized.* When requirements for a diverse product mix constrain the manufacturing process, additional considerations may dominate over those addressed in this article.

The present goal is to understand those aspects of the most expensive manufacturing step that dominate product cost. One corollary is to find approaches that minimize its contribution to this cost. Another corollary is to provide a focus on alternative processing routes that could circumvent this step. Important questions must be addressed. Among the most obvious are:

J. W. Halloran—contributing editor

Manuscript No. 191861. Received April 4, 1996; approved January 27, 1998.
*Member, American Ceramic Society.

Notation

a	thermal diffusivity of hot zone
A	numerical coefficient of order unity (Fig. C2)
A_0	reference area (1/3 m^2)
b	thickness of parts
B_O	parabolic oxidation coefficient
B_n	power reduction coefficient for radiation shields
c	oxygen concentration
c^*	reference oxygen concentration
c_O	initial oxygen concentration
c_p	specific heat
C_A	furnace acquisition cost
C_L	replacement cost for furnace constituents
$\dot{C}_x$	cost rate for floor space
d	grain diameter
D	gap thickness between parts
D_O	diffusivity for oxygen defect in AlN
f	furnace loading coefficient
$F(X)$	function governing evolution of physical property X
h	heat transfer coefficient
h_r	h for radiation
h_{nc}	h for natural convection
H	support thickness for hot zone
j	throughput
k	Boltzmann constant
k^*	reaction rate constant
K_c	fracture toughness of heating element material
l	heating element segment length
L	furnace length
n	power law creep exponent
N	number of parts per batch
p	partial pressure
P	power usage
Q	activation energy for thermally activated process
Q_c	Q for creep of heating element
Q_F	Q for furnace failure mechanism
Q_O	Q for oxygen diffusion through silicate
Q_p	Q for process that dominates property development
R	furnace hot zone radius
R_b	insulation radius
R_A	reference radius (1/3 m)
R_n	radius of radiation shields
R_o	outer wall radius
R_*	largest furnace size for high yield
s	ratio T_h/T_m
t	time
t_D	depreciation period for furnace acquisition
t_h	furnace heat-up time
t_L	furnace constituent lifetime
t_0	reference time for property kinetics
t_Q	reference time for cycle (3 h)
t_R	reference furnace lifetime (1000 h)
t_r	downtime for replacement and refurbishment
t_s	cycle time
t_s^*	firing time for furnace of radius R_*
t_{st}	downtime for stacking
t_Y	operating time per year
T	temperature
T_A	reference temperature (1000°C)
T_{max}	temperature at which a deleterious mechanism initiates
T_*	goal temperature for hot zone
T_c	temperature at center of hot zone
T_h	heating element temperature
T_m	temperature at outside of hot zone
T_M	melting temperature
T_o	furnace wall temperature
T_Q	temperature at which isothermal cycle time to reach $X = 0.9$ is t_Q
T_R	furnace "rating" temperature (Table I)
$\dot{T}$	heating rate
V_p	part volume
X	relative magnitude of physical property (ranges from 0 to 1)
X_0	initial value of X
X_{min}	minimum value of X according to product specifications
ΔX_{max}	maximum range in X according to product specifications
X_{max}	$X_{min} + \Delta X_{max}$, maximum value of X according to product specifications
Y	process yield (ranges from 0 to 1)
\$	cost per part
$\$_m$	contribution to \$ from raw-material price
$\$_1$	contribution to \$ from power use
$\$_2$	contribution to \$ from furnace acquisition
$\$_3$	contribution to \$ from replacement of furnace constituents
$\$_F$	cost coefficient for furnace acquisition
$\$_H$	cost coefficient for heating-element replacement
$\$_{MU}$	cost coefficient for muffle
$\$_s$	cost coefficient for support structure
$\Delta\$$	manufacturing cost per part: $\$_1 + \$_2 + \$_3$
α	cooling time proportionality constant (~1)
β	rating temperature exponent (~2)
$\dot{\gamma}$	strain rate
$\dot{\gamma}_0$	reference strain rate (3×10^{-6}/s)[12]
δ_I	insulation thickness
δ^*	critical creep displacement for short circuiting
ε	emissivity
ϕ_u	cost of electricity
η	furnace capacity fraction
κ	thermal conductivity
κ_I	κ for furnace insulation
κ_o	effective κ for furnace hot zone
κ_A	κ for AlN product
Λ	R^2/at_s
ρ	density
σ	Stephan–Boltzmann constant
$\bar{\sigma}$	stress
$\bar{\sigma}_0$	reference stress for creep (1 MPa)
ζ	coefficient related to number of radiation shields
ς	annual production

(i) Should continuous or batch processes be used?
(ii) What furnace construction should be used?
(iii) How large should the furnace be?
(iv) How rapidly should the heating and cooling be performed?
(v) What peak temperature should be used and how long should it be sustained?

Answering these questions and realizing this goal are facilitated by having thermal models for each high-temperature step. The level of modeling needs only be informative about the *trends and the scaling*. Coefficients in the models then require calibration before the cost analysis can be implemented.

Emphasis is given to batch processing, most relevant to the moderate annual production rates envisaged for market introduction strategies. Accordingly, the parts are installed in the furnace, which is then heated to the required temperature and cooled. In some cases, the parts can be raised and lowered into the furnace, which is maintained at a fixed temperature. The associated (lengthy) cycle time adds appreciably to the cost per part; however, the cost remains lower than that for continuous processes because of the lower capital expenditures. Vertical, bottom loading furnaces (Fig. 1) have been selected for this analysis because of their robustness in manufacturing against operating damage and their advantages in controlling yields, as elaborated below.

This article is organized in the following manner. In Section II, the basic cost framework is identified. In Section III, all of the parameters needed to complete the cost model are defined, and, in Section IV, simple steady-state scaling results are derived that offer initial insight about some of the more obvious trends. In Section V, a thermal analysis is performed that provides two essential relationships: the power requirements and the temperature gradients in the hot zone. In Section VI, furnace categories are outlined, and an assessment of acquisition and replacement costs is presented. In Section VII, furnace failure modes are examined and expressions given for the maximum operating temperatures, as well as the expected life. In Section VIII, the kinetics of property evolution are assessed and used to obtain expressions for the cycle time. In Section IX, yields are analyzed, and criteria for attaining high yields in batch operations are provided. Finally, in Section X, cost simulations are presented.

II. Technical Cost Framework

The basic cost formulation has the simple form[1–5]

$$\frac{\text{cost}}{\text{part}} = \text{material} + \frac{\sum_{\text{all}} \text{cost rate}}{\text{throughput}} \tag{1}$$

where

$$\text{throughput} = \frac{\text{number of parts}}{\text{cycle time}}$$

The summation is over all process steps. For each step, the contribution to the cost per part, \$, can be expressed from Eq. (1) as

$$\$ = \$_m + \frac{t_c}{N}\frac{\dot{C}_i}{Y} \tag{2}$$

where $\$_m$ is the price of the materials per part, t_c the cycle time, N the number of parts made in that cycle, Y the associated yield, and $\dot{C}_i$ a cost rate. For a high-temperature process step, $\dot{C}_i$ is given by

$$\dot{C}_i = P\phi_u + \frac{C_a}{t_D} + \sum_i \left(\frac{C_L}{t_L}\right) + \phi_\Lambda + \dot{C}_x \tag{3}$$

where P is the power requirement, ϕ_u the utility cost, C_a the acquisition cost for the high-temperature system, t_D the system's depreciation interval, C_L the cost of replacement furnace parts, and t_L their life expectancy, Σ_i the overall furnace constituents susceptible to failure, ϕ_Λ the labor rate, and $\dot{C}_x$ the cost rate for floor space. For present purposes, labor and floor-space costs are not considered. Their exclusion does not infer that they are unimportant. However, it recognizes that, once the throughput has been established and the other relevant times (t_L and t_D) determined, their contributions to \$ are straightforward to calculate. These costs must, of course, be included in the final cost determination for each product, as elaborated in Section X.

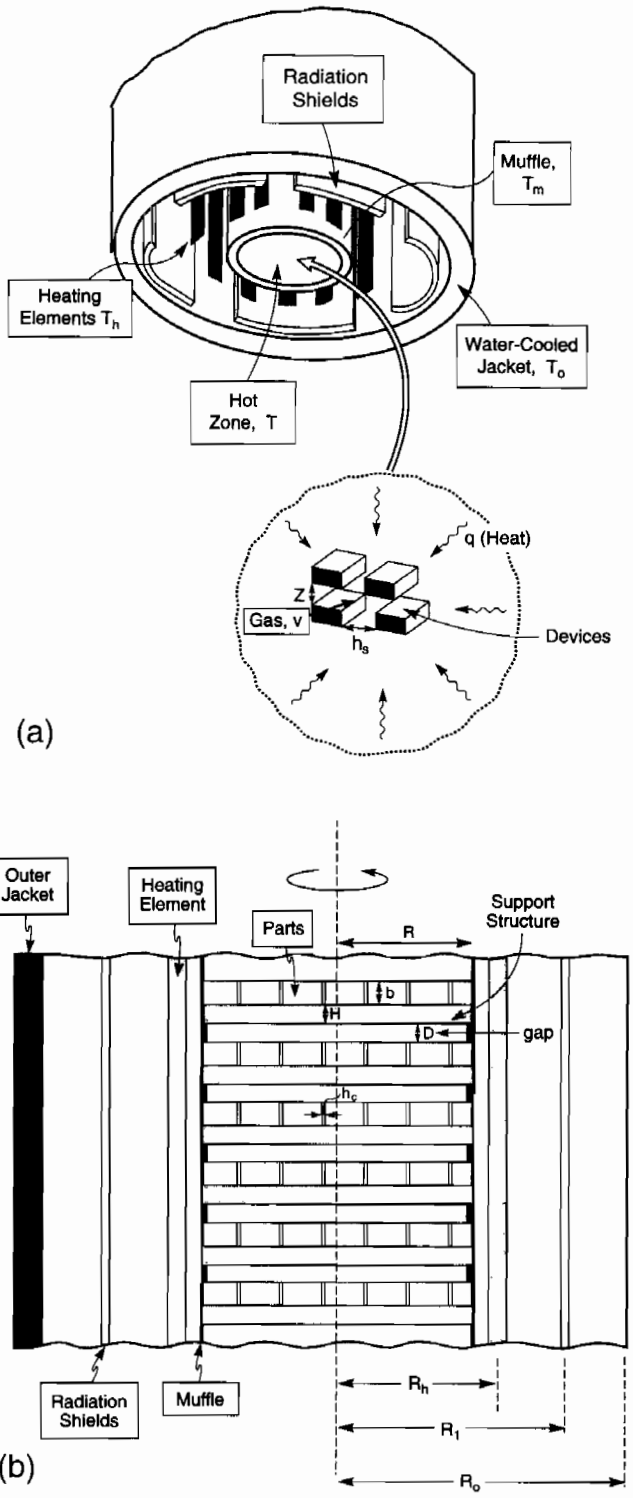

Fig. 1. Schematics of (a) the vertical cylindrical furnace and (b) the parts loading addressed by the analysis.

Equation (2) provides a basis for rephrasing the questions identified above.

(i) How does the goal temperature in the hot zone, T_*, affect each of the terms that contribute to the cost per part, and is there a temperature at which \$ has a minimum?

(ii) How does the furnace size or hot-zone capacity of radius R affect each term, and is there an optimum size?

(iii) Are there characteristics that define the influence of the hot zone design on \$?

It is shown that the salient hot zone characteristic is its effective thermal diffusivity, a.

Consequently, T_*, R, and a are the primary variables in the problem. Functions must be developed to simulate the costs and to find cost minima that relate these variables to the power, the cycle time, the acquisition costs, and the life expectancy. These functions are developed in the remainder of this article and then are used to perform cost simulations.

III. Parameter Definitions

The technical cost model (Eqs. (2) and (3)) contains nine different parameters that all interrelate. The challenge in formulating and implementing the model is to define relations between these parameters and the variables. Initially, this is done in the simplest manner that contains the essential mechanistic information: complexity always can be added. That is, first-order scaling relations are developed by inputting these parameters into Eqs. (2) and (3), subject to processes that operate predominantly in steady-state, with time-invariant, uniform temperatures in the hot zone. Subsequently, the crucially important effects of heat-up transients are incorporated.

The furnaces to be considered (Fig. 1(a)) comprise vertical, bottom-loading configurations with a cylindrical hot zone, circumvented by a muffle tube, heating elements, and an outer jacket. The furnace length is considerably larger than the outer radius, so that the end effects can be neglected. Consequently, the temperature does not vary along the active length. The parts to be processed in the furnace are considered to be small. They also are spaced closely to assure maximum throughput (Fig. 1(b)).

The three basic variables for such furnaces that affect the cost are the furnace hot zone radius, the operating temperature, and the price coefficient for the furnace construction materials. Functions are required that enable the parameters in Eq. (1) to be expressed in terms of these variables.

(1) Part Loading

The number of components per batch depends on the hot-zone radius, in accordance with

$$N = \frac{fR^2L}{V_p} \tag{3}$$

where L is the furnace length, V_p the volume of each component, and f a space-filling parameter. For a large number of small parts, f is in the range 0.3 to π, dictated by the support configuration.

(2) Cycle Time

The cycle time has several contributions. The first, t_s, requires elaboration. It represents that part of the manufacturing step needed to heat up the parts and hold them long enough to reach the property specification. When governed by a dominant, thermally activated mechanism operating in the body, this time is exponentially dependent on the temperature:

$$t_s \propto t_0 \exp\left(\frac{Q_p}{kT}\right) \tag{4a}$$

where Q_p is the activation energy, k the Boltzmann constant, and t_0 a reference time dictated by either a diffusion distance or a reaction-rate constant (Section VII). When more than one mechanism operates during the cycle, Eq. (4a) refers to that mechanism affording the *principal contribution* to t_s. Accordingly, Q_p and t_0 may be either mechanistic or empirical, as elaborated in Sections VIII and IX.

A property requirement must be introduced to develop Eq. (4a). X is defined for this purpose as that fraction of the realizable property of the product attained during the process cycle ($0 \leq X \leq 1$). Under isothermal conditions at temperature T, the property X develops with time such that

$$F(X) = \frac{t}{t_0} \exp\left(\frac{-Q_p}{kT}\right) \tag{4b}$$

The function $F(X)$ reflects the dependence of the property X on the thermally activated process. Several examples of this relation based on explicit mechanisms are derived in Section VIII. Throughout this article, we use the following normalization of Eq. (4b):

$$\frac{F(X)}{F(X_Q)} = \frac{t}{t_Q} \exp\left[\frac{Q_p}{k}\left(\frac{1}{T_Q} - \frac{1}{T}\right)\right] \tag{4c}$$

where t_Q and T_Q are reference values such that T_Q is the isothermal temperature required to bring the product to X_Q in time t_Q. (In subsequent numerical examples $t_Q = 3$ h and $X_Q = 0.9$.) The reference temperature, T_Q, can be either calibrated by experiment or obtained from models. It follows from Eq. (4c) that t_s is the time needed to achieve the property X at constant temperature, T:

$$t_s = t_Q \frac{F(X)}{F(X_Q)} \exp\left[\frac{Q_p}{k}\left(\frac{1}{T} - \frac{1}{T_Q}\right)\right] \tag{4d}$$

A second contribution to the cycle time is that needed to cool the furnace. This time is considered to be proportional to t_s with a proportionality constant α, or order unity. A third contribution, t_{st}, is the time needed to stack the parts between each production run. A fourth contribution is the downtime, t_r, needed to replace furnace constituents when they fail. These times combine in the manner elaborated below.

(3) Furnace Life

The life of the furnace parts, t_L, has a form similar to Eqs. (4), but with different activation energies and different reference times determined by failure mechanisms. These mechanisms are typically creep, oxidation, or fracture, as discussed in Section VII. The corresponding expression for the life under constant T conditions is

$$t_L = t_R \exp\left[\frac{Q_F}{k}\left(\frac{1}{T} - \frac{1}{T_R}\right)\right] \tag{5}$$

where t_R is the reference failure time at temperature T_R and Q_F the activation energy. Here, t_R is taken to be 1000 h and T_R is the maximum operating (or rating) temperature for the furnace (see Table I).

(4) Throughput

The throughput, j, based on one firing cycle, expressed as parts per unit time is

$$j = \frac{N}{(1+\alpha)t_s + t_{st}} \tag{6}$$

Table I. Summary of Furnace Parameters

Category	Elements	T_R (°C)	Q_F (kJ/mol)	$\$_A$ ($\times 10^3$ dollars)	$\$_H$ ($\times 10^3$ dollars)
I	Nickel(chromium)	1000	170	50	2
	SiC	1500	220	70	4
	$MoSi_2$	1700	130	70	4
II	Tungsten	1900	500	380	40
	Molybdenum	1600	350	380	30
	Tantalum	1500	280		
III	Graphite	2800		150	

The annual production, ζ, without downtimes for furnace repair, is $\zeta = jt_Y$, where t_Y is the operating time per year.

(5) Power Requirements

The power requirements depend on the temperature used to develop the properties and the furnace design. When T is large and radiation shields are used to lower the heat flux into the environment, the steady-state power (derived in Section V) scales as

$$P = \sigma\varepsilon RLT^4\zeta \tag{7a}$$

where σ is the Stephan–Boltzmann constant, ε the emissivity of the furnace constituents, and ζ a parameter of order unity that depends on the number, n, of radiation shields (see Eq. (14)). The corresponding result from Section V for a furnace that uses ceramic insulation to reduce the power is

$$P = \frac{2\pi T\kappa_I LR_0}{\delta_I} \tag{7b}$$

where δ_I is the insulation thickness, κ_I its thermal conductivity, and R_0 the outer wall radius.

(6) Acquisition Costs

Basic results for acquisition costs have been developed for the long, vertical, bottom-loading furnaces of present interest (Fig. 1). The three major scaling variables are the hot zone radius, the furnace length, and the "rating temperature" for the furnace, T_R. The latter represents the temperature above which the furnace has unacceptably short life for the reasons discussed in Section VII. This temperature is determined largely by the materials used to construct the heating elements, the insulation, the radiation shields, and the support structure.

The relations used are based on information provided by furnace vendors. In all cases, the costs vary linearly with the length, L. Otherwise, the following relation has been found to characterize acquisition for a wide range of furnaces, as discussed in Section V:

$$C_A = \frac{RL}{A_0}\left(\frac{T_R}{T_A}\right)^{\beta}\left[\$_A + \$_{MU} + \left(\frac{R}{R_A}\right)\$_s\right] \tag{8a}$$

where

$$\$_A = \$_F + \$_H \tag{8b}$$

and where A_0 is a reference area (1/3 m^2), T_A a reference temperature (1000°C), β an exponent larger than unity, and R_A a scaling radius (1/3 m). As elaborated in Section VI, the exponent $\beta \approx 2$. The price-scaling coefficients depend on the construction materials. The overall price, $\$_A$, is in the range \$70 000–\$400 000. The overall price includes the cost of the heating elements, $\$_H$, plus the furnace itself, $\$_F$. The latter incorporates the controller and the loading mechanism as well as other ancillaries (such as vacuum pumps, when necessary).

The coefficient $\$_{MU}$ refers to the muffle tube, when used. The coefficient $\$_s$ refers to the support structure. The structure cost scales with the hot zone volume. Information regarding this coefficient has not yet been acquired. It will be addressed in further studies.

(7) Replacement Costs

The corresponding result for the replacement of failed components can be obtained from Eq. (8) using the coefficients, $\$_H$, $\$_{MU}$, and $\$_s$. However, different lifetimes apply to each furnace constituent, so that these cost coefficients must be qualified by the appropriate t_L.

(8) Yields

The process yield, Y, is determined by material heterogeneity, by thermal gradients, and by gas-phase compositions. These issues are addressed in detail in Sections VIII and IX. Y is considered for preliminary scaling to be determined exclusively by material heterogeneity: typically of order unity.

IV. Scaling Relations

The following expression for the various contributions to the cost per part is derived under the assumption the furnace is operated at a constant temperature, T. Although this is clearly not the case, justification for its use as a scaling approximation is given in Section IX. Introducing Eqs. (3)–(8) into Eq. (2), with $Y \approx 1$ gives

$$\$ = \$_m + \Delta\$ \tag{9}$$

where

$$\Delta\$ = \$_1 + \$_2 + \$_3$$

$\$_m$ refers to material price, $\$_1$ to power costs, $\$_2$ to acquisition of the furnace, and $\$_3$ to replacements. The characteristics of each are as follows:

(i) The material cost is

$$\$_m = V_p\rho\$_{mat} \tag{10}$$

where ρ is the density and $\$_{mat}$ the price per kilogram for the material.

(ii) For a furnace with radiation shields, Eq. (7a) with Eqs. (3)–(5) gives

$$\$_1 = \frac{\sigma\varepsilon\zeta\phi_v t_Q T^4}{R\Delta_0}\exp\left[\frac{Q_p}{k}\left(\frac{1}{T} - \frac{1}{T_Q}\right)\right] \tag{11a}$$

where $\Delta_0 = f/V_p$. If the furnace has ceramic insulation,

$$\$_1 = \frac{2\pi\kappa_I\phi_u(R_0/\delta_I)t_Q T}{R^2\Delta_0}\exp\left[\frac{Q_p}{k}\left(\frac{1}{T} - \frac{1}{T_Q}\right)\right] \tag{11b}$$

(iii) The contribution from furnace acquisition is

$$\$_2 = \frac{\$_A(T_R/T_A)^2}{\Delta_0 RA_0 N_{DOWN} N_L} \tag{12a}$$

where N_L is the number of batches between downtimes ($N_L = t_L/t_s$), and N_{DOWN} the number of downtimes for furnace constituent replacement within the depreciation period, t_D, given by

$$N_{DOWN} = \frac{t_D}{N_L[(1+\alpha)t_s + t_{st}] + t_r} \tag{12b}$$

(iv) The cost associated with replacement of heating elements is

$$\$_3 = \frac{t_Q\$_H(T_R/T_A)^2[F(X)/F(X_Q)]}{t_R\Delta_0 RA_0}\exp\left[-\frac{Q_p}{k}\left(\frac{1}{T} - \frac{1}{T_Q}\right) + \frac{Q_F}{k}\left(\frac{1}{T} - \frac{1}{T_R}\right)\right] \tag{12c}$$

There are similar expressions for the failed support structure and muffles.

The total annual production (parts per year) accounting for downtime is

$$\zeta \equiv NN_L\frac{t_Y}{t_D}N_{DOWN} = \frac{(fR^2L/V_p)t_Y t_L}{\{N_L[(1+\alpha)t_s + t_{st}] + t_r\}t_s} \tag{12d}$$

These scaling rules provide the following straightforward cost implications. Recall, however, that transients, as well as mechanism transitions and other important effects not addressed in the steady-state analysis, have new implications.

(i) *Smaller components decrease all cost factors* by increasing the throughput.

(ii) *The higher the temperature, the smaller the power use cost contribution*; i.e., the temperature exponential in the cycle time (Eq. (4)) always dominates over the temperature dependence of the power (Eq. (7)). However, in most cases, there is

a temperature limit, corresponding to the temperature T_{max}, at which a transition to a deleterious mechanism occurs. This limit is discussed in Section X. The influence of temperature on $\$_2$ is contingent on the rating temperature, T_R. When $T << T_R$, $\$_2$ decreases as temperature increases, because of the effect of T on the cycle time (Eqs. (4) and (12*a*)). However, when T approaches T_R, a new construction material for the furnace is needed, and there is a *step function increase* in $\$_2$. Such considerations dominate the initial choice of the manufacturing method.

(iii) *Larger furnaces reduce all nonmaterial cost coefficients.* However, temperature gradients that result from bringing the furnace up to the goal temperature adversely influence the cycle time as the furnace size increases. The influence is manifest in the yield, through the property specifications described in Section IX. There also are limits set by furnace failure mechanisms, such as creep and fracture, and by the fabricability of the furnace construction materials, discussed in Section VI.

V. Furnace Models

(1) General Considerations

A thermal analysis is performed with two objectives:

(i) Establish expressions for the power required in steady-state operation, as functions of the hot zone temperature, T, its radius, R, and the insulation strategy (radiation shields or ceramic insulation).

(ii) Provide an approach for scaling temperature gradients, as well as power needs, during heat-up transients, as functions of the goal temperature, T_*; the ramp-up time, t_h; and R. Steady state is featured in the initial analysis for two related reasons: the expressions for the power facilitate scaling and the power demands in full operation are almost comparable to those for steady state.

Steady-state operation is defined in accordance with the following features. The temperature everywhere in the furnace is time independent. The hot zone temperature is spatially uniform and lower than that at the heating elements (Panel A). Such uniformity is applicable either when the elements are cylindrical and essentially continuous or when a thermally conductive muffle is used. When there are significant gaps between the elements and there is no muffle, a radiative flux through the gaps causes circumferential nonuniformities in the outer areas of the hot zone. The effects of these nonuniformities are not addressed here.

The parts are placed inside a muffle tube of emissivity ε_m (Fig. 1). Either multiple heat shields or insulation strategies are used to reduce the power requirements. The gases in the furnace are transparent, with no absorption and emission of radiation. The furnace has uniform, initial temperature. Elements, of radius R_h, having emissivity ε_h are heated by electric current. The outer surface temperature, T_o, is dictated by cooling.

Because the furnace contains many closely spaced parts (Fig. 1(b)), the flux within the hot zone is governed by conduction through the support structure and the parts, as well as by radiation across the gap. When the gap is narrow, the latter can be represented by an effective thermal conductivity, as elaborated in Panel A. Accordingly, the fluxes in the hot zone can be characterized by an effective thermal diffusivity, a, dictated by the parts, the support structure, and the gas flows (Panel A). In practice, this assertion needs to be assessed by calibration experiments performed on a prototypical furnace with the part loading appropriately scaled.

A furnace comprising radiation shields and a cooled outer wall is examined first, with the objective of determining the relation between the power, the temperature, the furnace radius, and the number of shields. A comparison is made between the heat flows caused by radiation and convection. A furnace with ceramic insulation then is considered, with the insulation thickness as the new variable.

(2) Steady State

(A) Radiation Heat Transfer: Radiation imposes a heat load on the furnace outer wall, with shields creating a resistance in the heat path. In steady state, with zero flux within the hot zone, the heat transfer between the heating element and shield 1 must be the same as that between shield 1 and shield 2, and so on. Thus, when thermal radiation is the *only heat exchange mechanism*[6–8] and there are n shields,

$$\frac{P_r(n)}{L} = \frac{2\pi R\sigma(T^4 - T_1^4)}{\frac{1}{\varepsilon} + \frac{R}{R_1}\left(\frac{1}{\varepsilon_i} - 1\right)} = \frac{2\pi R\sigma(T_1^4 - T_2^4)}{\frac{1}{\varepsilon_i} + \frac{R_1}{R_2}\left(\frac{1}{\varepsilon_i} - 1\right)} = \cdots = \frac{2\pi R\sigma(T_n^4 - T_o^4)}{\frac{1}{\varepsilon_i} + \frac{R_n}{R_0}\left(\frac{1}{\varepsilon_0} - 1\right)} \tag{13}$$

where P is the heat loss and σ the Stefan–Boltzmann constant. The transmissivity of the surfaces has been assumed to be zero in deriving Eq. (13) so that their reflectivity can be expressed as $1 - \varepsilon$.

The heat loss with multiple radiation shields and with prescribed temperatures, T and T_o is obtained from Eq. (13) as

$$\frac{P_r(n)}{L} = \frac{2\pi R\sigma(T^4 - T_o^4)B_n}{\frac{1}{\varepsilon} + \frac{R}{R_1}\left(\frac{1}{\varepsilon_i} - 1\right)} \tag{14a}$$

where n is the number of shields. Results for the coefficient B_n are given in Panel B. When normalized by the power use from a furnace with one radiation shield, the results depend only on n (Fig. 2(c)). The following simple approximation is obtained as a fit to the full numerical results:

$$\zeta = \frac{P_r(n)}{P_r(1)} \approx 1.35\ \exp(-b_r n) \tag{14b}$$

where $b_r \approx 0.3$. Tungsten is much less effective than molybdenum in retarding the overall heat loss, because its emissivity is typically 3 times larger.[6] Graphite, with an even larger emissivity ($\varepsilon \approx 0.8$), requires considerably more power.

(B) Natural Convection: Within the annulus between two vertical concentric cylinders, radii R_1 and R_2, having isothermal wall temperatures T_1 and T_2, convection cells affect the heat transfer, such that the radial heat flux is[6–8]

$$\frac{P_{nc}}{L} = \frac{2\pi(T_1 - T_2)\kappa_e}{\ln(R_2/R_1)} \tag{15}$$

where the effective thermal conductivity of the gas, κ_e, is related to the Nusselt Number, Nu, by[6] $\kappa_e = \kappa_g Nu$, where κ_g is the actual thermal conductivity of the gas. For most furnaces,

$$Nu = 0.073(Ra)^{1/3} \tag{16}$$

where Ra is the Rayleigh number,

$$Ra = \frac{g\beta_g(T_1 - T_2)(R_2 - R_1)^3}{\alpha_g \nu_g}$$

where g is the gravitational acceleration, β_g the coefficient of thermal expansion for the gas, ν_g the kinematic viscosity of the gas, and α_g the thermal diffusivity of the gas.

The overall heat flux associated with radiation and natural convection is

$$P = P_r + P_{nc} = 2\pi(T_1 - T_2)h_r\left(1 + \frac{h_{nc}}{h_r}\right) \tag{17}$$

Panel A. Fluxes in the Hot Zone

Thermal transport into the hot zone is clearly a critical factor in controlling the yields and the cycle times. There are numerous possible scenarios involving conduction, convection, and radiation that depend on the overall geometry and the manner in which the devices are loaded into the furnace. The parts loading and the materials are the crucial factors for a long cylindrical furnace dominated by radial heat fluxes. As a beginning, a construct is used that represents the batch processing of relatively small devices where gas dynamics are of secondary importance. The role of gas flows is considered elsewhere. In such cases, for high throughput and lowest cost, the parts are loaded into the hot zone as close to one another as possible. The schematic on Fig. 1(b) is intended to visualize this situation. The principal consequence is that the gaps between the support structure and the devices are small, with implications for the role of radiation. That is, radiation can enter only through these narrow gaps and propagate along the gap by internal reflections.

The use of a muffle tube is considered because of its benefit in equilibrating the temperature at the outer diameter of the hot zone. Although this adds to acquisition and replacement costs, it increases the yields. Here, the latter is assumed to have the larger effect, with an overall lower cost per part (relative to a furnace without a muffle). This choice enables the temperature upon heat up to be controlled at the muffle and used as a means for assuring high yields in accordance with the arguments presented in Section IX.

The temperature distribution for this scenario can be represented by the effective thermal diffusivity, a, as used in the text and elaborated below. Accordingly, measurements of temperature made on a prototypical furnace should scale with radius in a manner consistent with Eq. (20*b*). Such measurements constitute the essential test. A coarse estimate of the diffusivity is made using a composite model. In practice, the diffusivity needs to be measured for the furnace and parts loading to be used in manufacturing. The principal flux comprises conduction along the support structure. The parts tend to have a very low conductivity because of porosity and small intrinsic material conduction. Consequently, heat conducts into the hot zone through the supports and then diffuses upward into each individual device (as well as downward from the radiation). When the devices are small (thin), relative to the hot zone radius, they rapidly equilibrate their temperature to that of the underlying support material. Supports are typically made from SiC, Al_2O_3, or refractory metals. All of these materials exhibit conductivities that decrease with increase in temperature. The conductivities, κ_s, at high temperature are[1,8] 5–20 W/(m·K) for ceramics and 30–80 W/(m·K) for refractory metals.

If the radiative flux is ignored and the conduction occurs only through the supports, the effective conductivity is simply

$$\kappa_o = \nu_s \kappa_s \tag{A–1}$$

with

$$\nu_s = \frac{H}{H + D + b}$$

where H is the thickness of the supports, b the thickness of the parts, and D the gap size (Fig. 1(b)). Typically, ν_s is ~0.2, giving κ_o of order 1–20 W/(m·K).

The effect of the gap can be characterized by an equivalent conductivity κ_g dominated by radiation and approximated by[25]

$$\kappa_g \approx \frac{\sigma R (T_m^2 + T_c^2)(T_m + T_c)}{\frac{1}{\mathcal{R}} + 2\left(\frac{1}{\varepsilon} - 1\right)} \tag{A–2}$$

where ε is the emissivity of the surface and $\mathcal{R}$ the radiation factor that depends on geometry. For a parallel plate configuration with a narrow gap, the data in Jacob[26] suggest that

$$\mathcal{R} \approx 0.65 \left(\frac{D}{R}\right)^{1/3} \tag{A–3}$$

Inserting some typical values leads to the range plotted on Fig. A1. Clearly, radiation can be as important as conduction at the higher temperatures. When it is significant, this contribution to the effective conductivity can be included by using

$$\kappa_o = \nu_s \kappa_s + \nu_g \kappa_g \tag{A–4}$$

where

$$\nu_g \approx \frac{D}{D + H + b}$$

The muffle temperature, T_m, is used here because the control surface differs from the heating element temperature, T_h (which controls the power and the element life), by a factor s, dictated by the geometric configuration:

$$T_h = sT_m \tag{A–5}$$

When the heating elements are cylindrical, with radius r_h and separation h, heat transfer is dictated by radiation:

$$s \approx \left(\frac{h}{2r_h\varepsilon}\right)^{1/4} \tag{A–6}$$

This factor is typically of order 1.1–1.3.

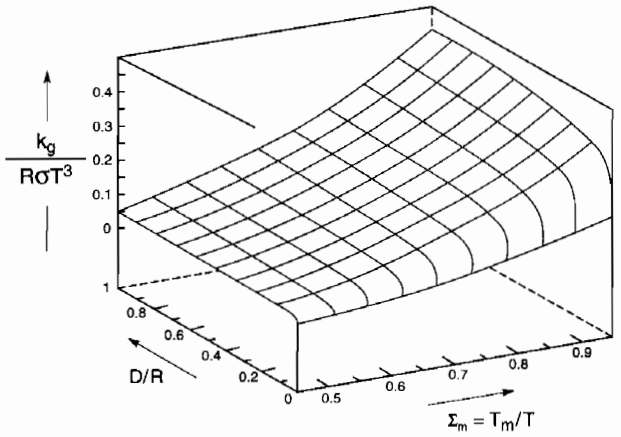

Fig. A1. Effective gas-phase thermal conduction caused by radiation, as a function of the gap size.

Panel B. Coefficients for Heat Transfer Functions

The coefficient B_n in Eq. (14) is determined according to the following results. For $n \leq 3$,

$$B_1 = (1 - A_1), B_2 = \frac{\prod_{i=1}^{2}(1 - A_i)}{1 - (1 - A_1)A_2}, B_3 = \frac{\prod_{i=1}^{3}(1 - A_i)}{1 - (1 - A_1)A_2 - (1 - A_2)A_3} \tag{B–1}$$

For $n > 3$,

$$B_k = \frac{(1 - A_k)}{\frac{1}{B_{k-1}} + \frac{D_k}{\prod_{i=1}^{k-1}(1 - A_i)}} \tag{B–2}$$

When there is only one radiation shield ($n = 1$),

$$A_1 = \frac{\frac{1}{\varepsilon_i} + \frac{R_1}{R_o}\left(\frac{1}{\varepsilon_o} - 1\right)}{\left(\frac{2}{\varepsilon_i} - 1\right) + \frac{R_1}{R}\frac{1}{\varepsilon} + \frac{R_1}{R_o}\left(\frac{1}{\varepsilon_o} - 1\right)} \tag{B–3}$$

The corresponding A_i coefficients for $n > 1$ are

$$A_1 = \frac{\frac{1}{\varepsilon_i} + \frac{R_1}{R_2}\left(\frac{1}{\varepsilon_i} - 1\right)}{\left(\frac{2}{\varepsilon_i} - 1\right) + \frac{R_1}{R}\frac{1}{\varepsilon} + \frac{R_1}{R_2}\left(\frac{1}{\varepsilon_i} - 1\right)} \tag{B–4}$$

and, for $k = 2, 3, \ldots, (n - 1)$,

$$A_k = \frac{\frac{1}{\varepsilon_i} + \frac{R_k}{R_{k+1}}\left(\frac{1}{\varepsilon_i} - 1\right)}{\left(\frac{2}{\varepsilon_i} - 1\right) + \frac{R_k}{R_{k-1}}\frac{1}{\varepsilon} + \frac{R_k}{R_{k+1}}\left(\frac{1}{\varepsilon_i} - 1\right)}$$

The coefficients D_k appearing in B_k when $6 \geq k > 3$ are given by

$$\begin{aligned} D_4 &= -(1 - A_3)A_4 + (1 - A_1)(1 - A_3)A_2A_4 \\ D_5 &= -(1 - A_4)A_5 + (1 - A_2)(1 - A_4)A_3A_5 \\ &\quad + (1 - A_1)(1 - A_4)A_2A_5 \\ D_6 &= -(1 - A_5)A_6 + (1 - A_3)(1 - A_5)A_4A_6 \\ &\quad + (1 - A_2)(1 - A_5)A_3A_6 + (1 - A_1)(1 - A_5)A_2A_6 \\ &\quad + (1 - A_1)(1 - A_3)(1 - A_5)A_2A_4A_6 \end{aligned} \tag{B–5}$$

The results for D_k when $k > 6$ contain lengthy expressions and, hence, are omitted for brevity.

The radiation shield temperature can be rewritten as a fourth-order governing equation with T_1 the only unknown:

$$T_1^4 + c_1T_1 + d_1 = 0 \tag{B–6}$$

where the coefficients c_1 and d_1 are given below. The solution to Eq. (B–6) must be bounded by T and T_o and is found to be

$$T_1 = \frac{\sqrt{2}}{2}\left(-p + \sqrt{\frac{c_1}{p} - p^2}\right) \tag{B–7}$$

where

$$p^2 = \left[\frac{c_1^2}{16} + \sqrt{\left(\frac{c_1^2}{16}\right)^2 - \left(\frac{d_1}{3}\right)^3}\right]^{1/3} - \left[-\frac{c_1^2}{16} + \sqrt{\left(\frac{c_1^2}{16}\right)^2 - \left(\frac{d_1}{3}\right)^3}\right]^{1/3}$$

The coefficients for Eq. (B–6) are,

$$c_1 = \frac{a_3 + a_4}{a_1 + a_2}$$

$$d_1 = -\frac{a_1T^4 + a_2T_o^4 + a_3T + a_4T_o}{a_1 + a_2} \tag{B–8}$$

with

$$a_1 = \frac{\sigma R_1}{\frac{1}{\varepsilon_i} + \frac{R_1}{R}\left(\frac{1}{\varepsilon} - 1\right)}$$

$$a_2 = \frac{\sigma R_o}{\frac{1}{\varepsilon_o} + \frac{R_o}{R_1}\left(\frac{1}{\varepsilon_i} - 1\right)}$$

$$a_3 = \frac{\kappa_e^-}{\ln\frac{R_1}{R}}$$

$$a_4 = \frac{\kappa_e^+}{\ln\frac{R_o}{R_1}}$$

When the furnace is insulated, the equation governing the temperature T_b is

$$T_b^4 + \left(\frac{f_1}{f_2}\right)T_b - \left(T_b + \frac{f_1}{f_2}T_o\right) = 0 \tag{B–9}$$

where the coefficients f_1 and f_2 are given below. The solution to T_b that satisfies both Eq. (B–9) and the condition $T > T_b > T_o$ is given by

$$T_b = \frac{\sqrt{2}}{2}\left(-q + \sqrt{\frac{c_2}{q} - q^2}\right) \tag{B–10}$$

where

$$q^2 = \left[\frac{c_2^2}{16} + \sqrt{\left(\frac{c_2^2}{16}\right)^2 - \left(\frac{d_2}{3}\right)^3}\right]^{1/3} - \left[-\frac{c_2^2}{16} + \sqrt{\left(\frac{c_2^2}{16}\right)^2 - \left(\frac{d_2}{3}\right)^3}\right]^{1/3}$$

with $c_2 = f_1/f_2$ and $d_2 = -(T^4 + c_2T_o)$. The coefficients for Eq. (B–9) are

$$f_1 = \kappa_1\left[\frac{1}{\varepsilon_i} + \frac{R_1}{R_b}\left(\frac{1}{\varepsilon_b} - 1\right)\right]\left[\sigma R_1 \ln\frac{R_o}{R_b}\right]^{-1}$$

$$f_2 = \left[\frac{1}{\varepsilon_i} + \frac{R_1}{R_b}\left(\frac{1}{\varepsilon_b} - 1\right)\right]\left[\left(\frac{1}{\varepsilon_i} - 2\right) + \frac{R_1}{R}\frac{1}{\varepsilon} + \frac{R_1}{R_b}\left(\frac{1}{\varepsilon_b} - 1\right)\right]^{-1} \tag{B–11}$$

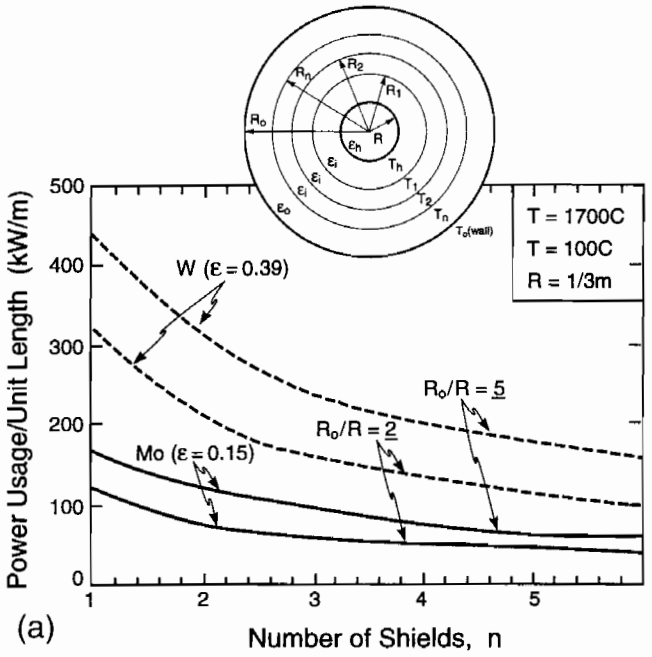

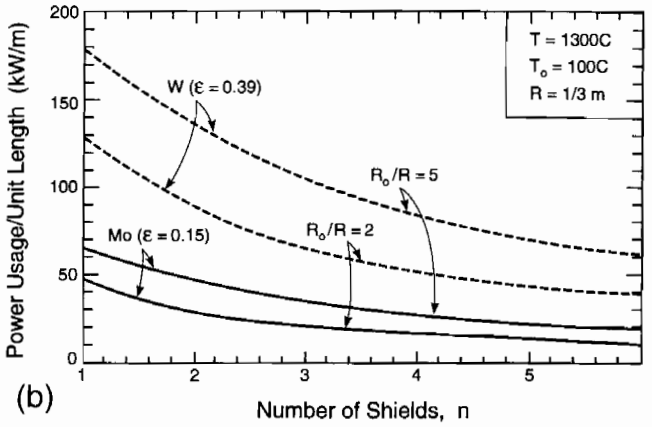

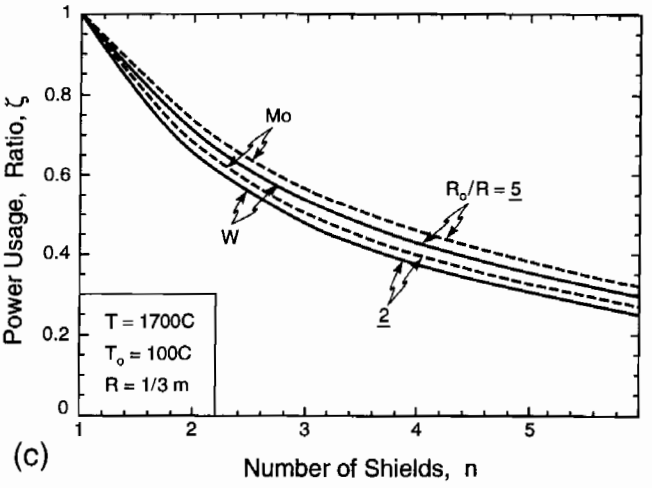

Fig. 2. Power use per unit length as a function of the number of radiation shields: (a) 1700°C hot zone, (b) 1300°C hot zone, and (c) normalized by P for one shield (hot zone, R = 1/3 m, and outer wall temperature, T_o = 100°C).

where the heat transfer coefficients are obtained from Eqs. (14) and (16) as

$$h_r = \frac{\sigma R_1 (T_1 + T_2)(T_1^2 + T_2^2)}{\dfrac{1}{\varepsilon_1} + \dfrac{R_1}{R_2}\left(\dfrac{1}{\varepsilon_2} - 1\right)}$$

and

$$h_{nc} = 0.073 \kappa_g \frac{(R_2 - R_1)}{\ln (R_2/R_1)} \left[g\beta_g \frac{(T_1 - T_2)}{\nu_g \alpha_g} \right]^{1/2}$$

The walls are at a much lower temperature than either the heating elements or the radiation shields, whereupon $T_2 << T_1$. Hence, the heat transfer ratio reduces to

$$\frac{h_{nc}}{h_r} \approx \frac{0.073(\kappa_g/\sigma\varepsilon)(g\beta_g/\nu_g\alpha_g)^{1/3}(R_2/R_1)}{T_1^{8/3} \ln (R_2/R_1)} [1 - (R_1/R_2)^2] \quad (18)$$

A plot of h_{nc}/h_r as a function of temperature for a nitrogen-gas atmosphere (Fig. 3) indicates that convection generally can be neglected when the hot zone temperature exceeds ~1300°C, whereupon Eq. (14) is the requisite expression for the power. Otherwise, both contributions must be considered, and Eq. (17) is needed to account for the power demands.

(C) Insulated Furnace: If a furnace has an insulated outer wall, temperature T_b, radius R_b, and a single radiation shield, at temperature T_1, heat balance subject to a high heat-transfer coefficient at the surface yields[6–8]

$$\begin{aligned} \frac{P_1}{L} &= \frac{2\pi R \sigma (T^4 - T_1^4)}{\dfrac{1}{\varepsilon} + \dfrac{R}{R_1}\left(\dfrac{1}{\varepsilon_i} - 1\right)} \\ &= \frac{2\pi R_1 \sigma (T_1^4 - T_b^4)}{\dfrac{1}{\varepsilon_i} + \dfrac{R_1}{R_b}\left(\dfrac{1}{\varepsilon_b} - 1\right)} \\ &= \frac{2\pi \kappa_o (T_b - T_o)}{\ln \dfrac{R_o}{R_b}} \end{aligned} \quad (19)$$

The temperature of the insulation is derived in Panel A, enabling the effects of insulation thickness, $\delta_1 = R_o - R_b$, to be determined (Fig. 4). Here, the insulation material is taken to have a thermal conductivity, κ_0 = 0.5 W/(m·K), representative of porous or fibrous ceramics.[1,8] There is a dramatic reduction in the power use as the insulation thickness increases, comparable to a multiple-radiation-shield furnace with no insulation (Fig. 2). T_b is considerably higher that T_o and about equal to T

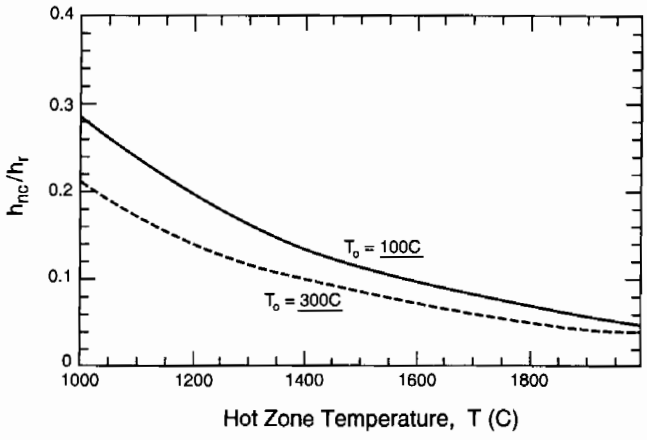

Fig. 3. Relative effects of conduction and radiation on the heat-transfer coefficients.

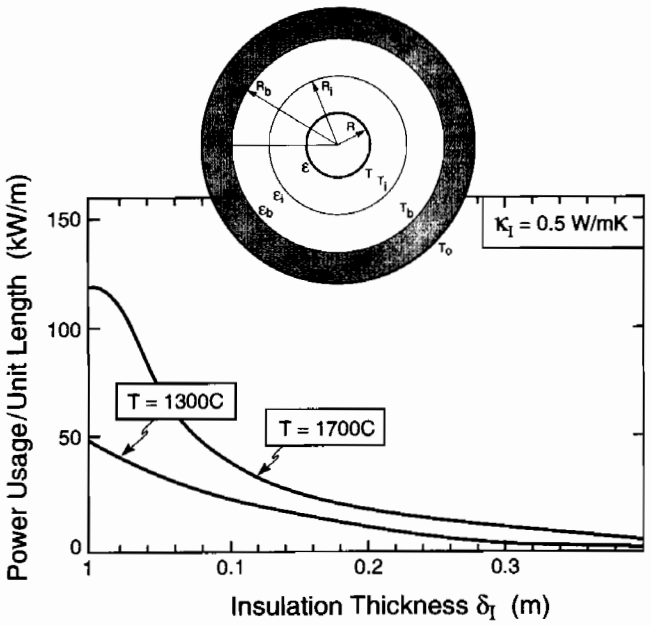

Fig. 4. Power use per unit length for a furnace with ceramic insulation.

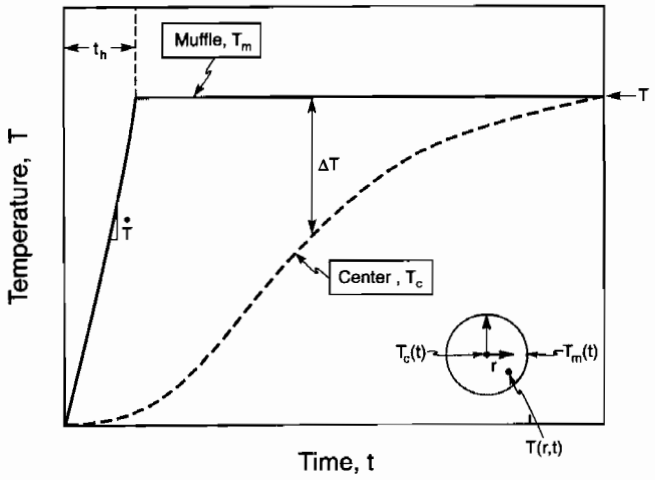

Fig. 5. Schematic illustrating the radial temperature distribution upon heat up within a long cylindrical furnace (see Fig. 1).

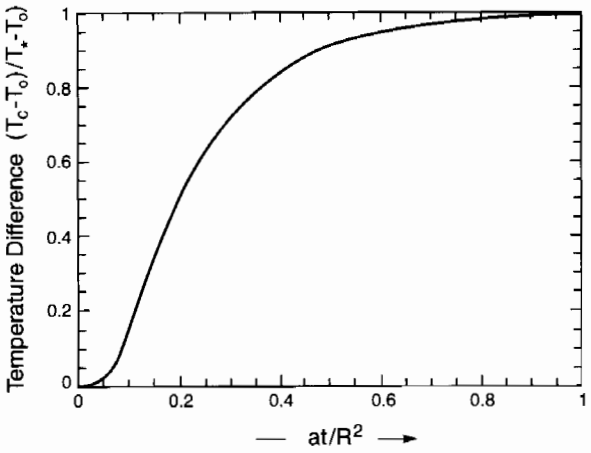

Fig. 6. Effects of nondimensional heat-up time at/R^2 on the temperature difference between the muffle and the hot zone center.

when the insulation is thick enough to cause a beneficial decrease in the power. Accordingly, in a well-designed furnace, the power demands given by Eq. (19) can be approximated by replacing T_b with T.

(3) Temperature Gradients in the Hot Zone

There are temperature gradients in the hot zone during the heating transient (see Fig. 5). Expressions for these gradients are derived for conductive flow with temperature control imposed at the muffle or, equivalently, at the outer diameter of the hot zone. Then, the gradients can be explicitly determined by considering only the inward heat flows. The outward flows determine the power requirements. The differential equation governing inward heat flow controlled by conduction is[6,9]

$$\frac{\partial^2 T}{\partial r^2}+\frac{1}{r}\frac{\partial T}{\partial r}=\frac{1}{a}\frac{\partial T}{\partial t} \tag{20a}$$

where r is the distance from the center (see Fig. 5) and a the effective thermal diffusivity of the hot zone (Panel A).

Representations exist for the solution to Eq. (20*a*) under temperature histories prescribed at $r = R$.[6,9] A special case of interest is a hot zone at uniform initial temperature, T_0, at $t = 0$, with the temperature at the outer perimeter ($r = R$) increased abruptly to the goal temperature, T_*, and subsequently held constant. The interior temperature lags that at the perimeter, with the temperature at the center, T_c, being the lowest. The temperature increase at the center of the hot zone relative to that at the perimeter is given by

$$\frac{T_c-T_0}{T_*-T_0}=1-\sum_{n=1}^{\infty}c_n\ \exp\left(-\omega_n^2\frac{at}{R^2}\right) \tag{20b}$$

where the first four values of c_n are 1.6020, −1.0648, 0.8514, and −0.7296 and of ω_n are 2.405, 5.520, 8.654, and 11.792. (The infinite sum equals unity for $t = 0$.) The nondimensional time variation from Eq. (20*b*) is plotted in Fig. 6. The expected range for R^2/a needs to be identified to address the time for T_c to approach T_*. Furnace radii lie between 1/10 and 1 m (Sections VI and X), whereas the effective thermal diffusivity (Panel A) is in the range 10^{-6}–10^{-5} m^2/s. Thus, the catch-up time (which scales with R^2/a) can be as short as an hour or as long as several days.

The size of the furnace must be chosen such that the product at the center attains property goals that differ from those at the perimeter by no more than a specified amount. An analysis leading to a specific choice is given in Panel C, and the result is presented in Section IX.

(4) Power Usage

Analysis of the temperature evolution and heat flow outside the muffle is needed for calculating the power supply to the heating elements. The result is

$$P(t)=\frac{2\pi R_h\sigma(T_h^4-T_m^4)}{\frac{1}{\varepsilon_h}+\frac{R_h}{R}\left(\frac{1}{\varepsilon_m}-1\right)}+\frac{2\pi\kappa_e^{(1)}(T_h-T_m)}{\ln\frac{R_h}{R}}$$
$$+\frac{2\pi R_0\sigma(T_h^4-T_0^4)}{\frac{1}{\varepsilon_o}+\frac{R_0}{R_h}\left(\frac{1}{\varepsilon_h}-1\right)}+\frac{2\pi\kappa_e^{(2)}(T_h-T_o)}{\ln\frac{R_0}{R_h}} \tag{21}$$

where the first two terms refer to the inward flows from the elements to the muffle, and the remaining two represent the outward flow (Panel B). Numerical results are plotted on Fig. 7 for selected values of hot zone conductivity, which determines $T_h(t)$. Typically, a power surge is needed at the beginning to achieve a constant heating rate at the muffle. The excess power is needed because of the flux drawn into the hot zone. However, the power requirements soon diminish toward

Panel C. Furnace Size for Specified Properties

The objectives stated in Eqs. (34) and (35) require that the properties of the product lie between X_{min} and $X_{max} = X_{min} + \Delta X_{max}$. The cylindrical furnace is considered long enough such that end effects can be neglected. Gradients in the axial direction are ignored. The initial temperature at $t = 0$ is T_0. As discussed in Section IX, a good estimate of the largest efficient furnace is provided by the determination of the hot zone size for which the outer perimeter temperature is increased directly to the goal temperature, T_*, simultaneously achieving X_{min} at the center and X_{max} at the perimeter when $t = t_s^*$. Because the temperature is constant at T_* on the perimeter (at $r = R$), the relation between t_s^* and $F(X_{max})$ from Eq. (26*c*) is that given in Eq. (38).

The temperature history at the center of the hot zone, T_c, is given by Eq. (20*b*). The radius $R = R_*$ such that $F = F(X_{min})$ at the center at $t = t_s^*$ is sought. By Eq. (26*c*), this condition is

$$F(X_{min}) = F(X_Q) t_Q^{-1} \int_0^{t_s^*} \exp\left[\left(\frac{Q_p}{k}\right)\left(\frac{1}{T_Q} - \frac{1}{T_c}\right)\right] dt \tag{C–1}$$

Combining Eqs. (38) and (C–1), this condition can be rewritten as

$$\frac{F(X_{min})}{F(X_{max})} = \Lambda \int_0^{1/\Lambda} \exp[-qf(\xi)]\, d\xi \tag{C–2}$$

where $q = Q_p/aT_*$, $\Lambda = R_*^2/at_s^*$, and

$$f(\xi) = \frac{(T_* - T_0)\sum_{n=1}^{\infty} c_n \exp(-\omega_n^2 \xi)}{T_* - (T_* - T_0)\sum_{n=1}^{\infty} c_n \exp(-\omega_n^2 \xi)} \tag{C–3}$$

The function $f(\xi)$ derives from the solution of Eq. (20*b*) for the temperature at the center.

Numerical evaluation of $F(X_{min})/F(X_{max})$ as a function of Λ using Eq. (C–2) reveals that the dependence is essentially linear in Λ for values of $F(X_{min})/F(X_{max})$ between 1/2 and 1 (Fig. C1). An asymptotic expansion of Eq. (C–2) for small Λ can be performed to obtain the coefficient of the linear term in Λ. As Λ becomes small, $(1 - T_0/T_*)c_1 \exp(-\omega_n^2 \xi)$ is the only term from $f(\xi)$ that makes a contribution to Eq. (C–2). With this substitution in Eq. (C–2), evaluation of the resulting integral for small Λ gives

$$\frac{F(X_{min})}{F(X_{max})} = 1 - \Lambda A(z) \tag{C–4}$$

where

$$A(z) = \frac{\gamma + \ln(z) + E_1(z)}{\omega_1^2}$$

and

$$z = c_1 \frac{Q_p}{kT_*}\left(1 - \frac{T_0}{T_*}\right) \tag{C–5}$$

Here, $\gamma = 0.57722$ (Euler's constant), $c_1 = 1.602$, $\omega_1 = 2.405$, and

$$E_1(z) = \int_z^{\infty} t^{-1} \exp(-t)\, dt$$

which is the exponential integral. Numerical values of A are plotted on Fig. C2, which shows that A depends only weakly on z and is within the range 0.6–1 for systems of interest.

In summary, with $R = R_*$, Eq. (C–4) provides the size of the furnace, given the desired property limits specified by X_{min} and X_{max}, assuming that $F(X_{min})/F(X_{max})$ is not less than about 1/2. The result is given in the text (Eq. (39)).

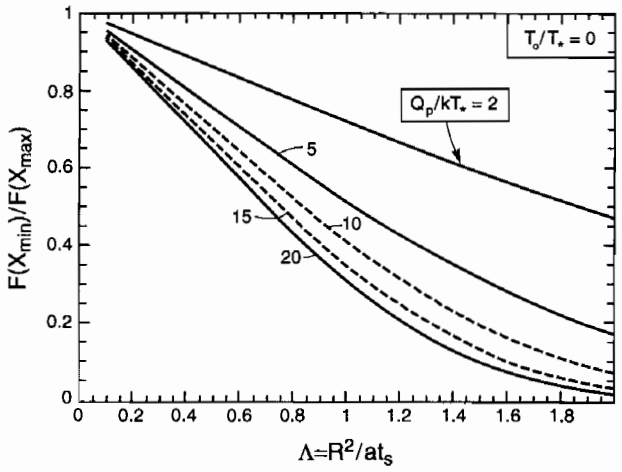

Fig. C1. Property ratio (maximum to minimum) as a function of the nondimensional furnace size for various activation energies.

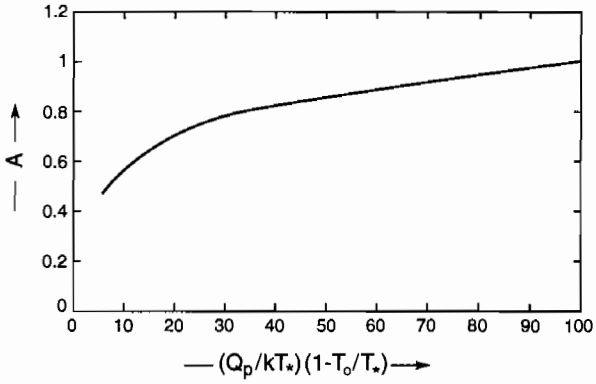

Fig. C2. Activation energy coefficient, A, for at the cost minimum.

a constant level, given by the steady state, well before the end of the heating cycle.

VI. Furnace Constructions

Decisions about the design and operation of the furnace involve interplays between cycle time, furnace capacity, and constituent failure modes, as affected particularly by the construction materials. The basic furnace construction depends upon the gas-phase and temperature requirements in the hot zone, with important consequences for cost. That is, when stringent controls are imposed on the gas phase to satisfy product performance specifications at high yield, furnace design becomes paramount.

In the absence of first-principles methods for determining furnace costs, the following strategy has been adopted. Infor-

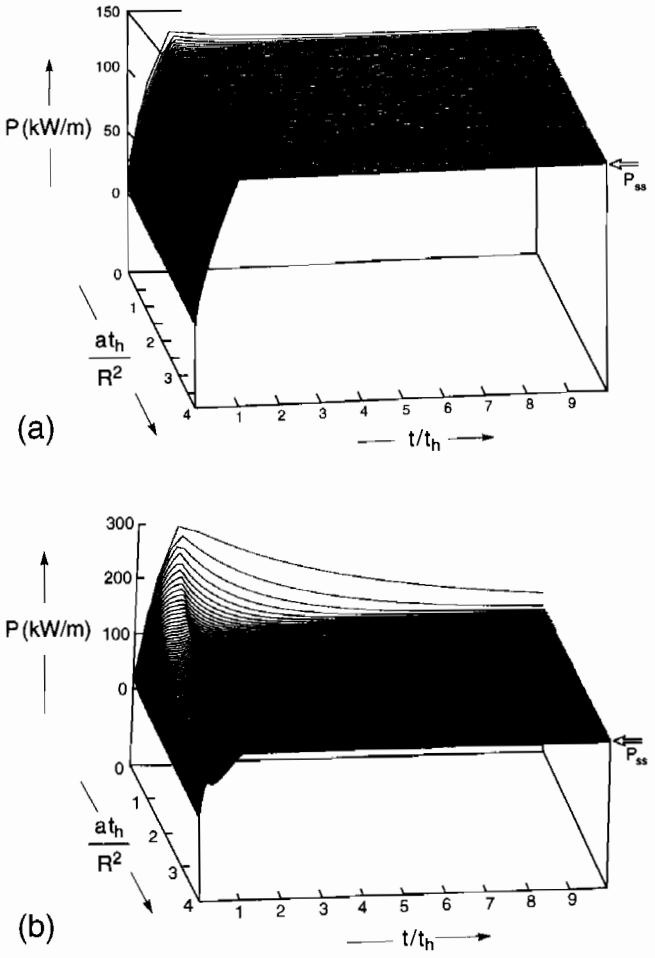

Fig. 7. Power requirement for attainment of a specified heat-up rate at the elements, plotted for two levels of the hot zone thermal conductivity: (a) κ_o = 1 W/(m·K) and (b) κ_o = 20 W/(m·K).

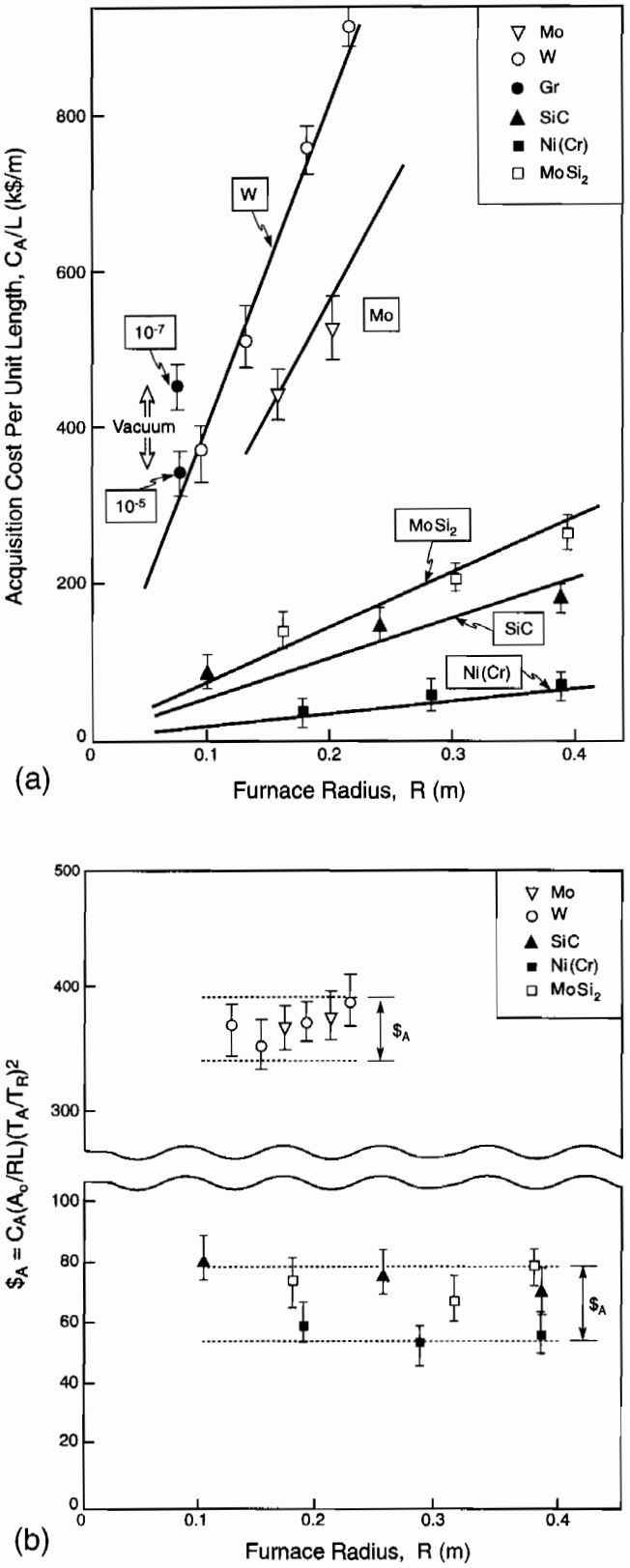

Fig. 8. Aquisition costs for furnaces as a function of hot zone radius: (a) cost per unit length and (b) size-normalized cost.

mation about purchase prices has been obtained from a range of vendors. These prices have been analyzed for the three constructions described below (Table I). Such analysis has revealed that, for purposes of cost simulation, the information can be expressed in accordance with Eq. (8):

$$C_A \approx \frac{RL}{A_0}\left(\frac{T_R}{T_A}\right)^{\beta}(\$_F + \$_H) \tag{22}$$

There is a direct scaling of C_A with the length, L, because short furnaces are combined to form longer furnaces. The price appears to scale about linearly with the hot zone radius, R, because of the increase in the amount of material needed. There is a major influence of the construction materials, reflected in the rating temperature, T_R. That is, the higher T_R, the greater the price, because more-costly materials are needed. This trend can be characterized by a power-law dependence on T_R, with exponent $\beta \approx 2$. For implementation in the cost model, the terms in Eq. (22) are nondimensionalized as RL/A_0 and T_R/T_A, where A_0 is taken to be 1/3 m^2 and T_A as 1000°C (T_R is measured in degrees celcius in Eq. (22)). Then, the coefficient $\$_A$ is only a function of the construction category, described next. A summary is given in Table I.

Category I furnaces are constructed with $MoSi_2$, SiC, or nickel(chromium) heating elements and ceramic insulation. They are the least expensive and operate with air as the environment around the elements. Vendor information for these furnaces (Fig. 8) when fit to Eq. (8) or Eq. (22) gives $\$_A \approx$ $70 000. Their rating temperatures range from ~1000°C for nickel to 1700°C for $MoSi_2$, governed by either creep or oxidative weakening. The activities of vapor phases are controlled using a ceramic muffle tube. But control is often difficult for vapor-phase-sensitive processes, with adverse effects on the yields. In such cases, it can be more cost effective to use category II or III furnaces, as discussed in Section X.

When a muffle is needed, it typically is made from a ce-

ramic, usually Al_2O_3 or SiC. These are susceptible to failure by thermal shock and creep. Preliminary information has been obtained on the cost of Al_2O_3 muffles. The rating temperature is based on creep and is dependent on purity. For a grade with $T_R \approx 1400°C$, a fit to Eq. (8) gives $\$_m \approx \$1000$. But, there is an upper size limit (~0.25 m) set by the capacity for extruding or casting the material.

A category II furnace with refractory-metal hot zone constituents, radiation shields, and water-cooled steel jacket may be preferred for processes requiring low oxygen partial pressure and low carbon activity. Such furnaces are relatively expensive. Nevertheless, a wide cost range exists, and category II furnaces may be preferred, as found in Section X. For these furnaces, vendor data give the acquisition costs plotted on Fig. 8, with $\$_A \approx \$380\,000$. The rating temperatures are limited by creep and range from ~1500°C for tantalum to 1900°C for tungsten.

When high temperatures and low oxygen pressures are required, but large carbon activities are acceptable, a category III graphite hot zone construction is feasible, in conjunction with a water-cooled steel jacket and radiation shields. The furnace designs are similar to those used with refractory metals, and the acquisition costs are similar. The operating temperature is limited only by the oxygen partial pressure, such that 2500°C can be realized at low oxygen levels. Using this temperature as T_R, the price coefficient is $\$_A \approx \$150\,000$.

The replacement costs for heating elements naturally scale with *RL*, but again increase as the rating temperature increases, such that a power-law function with $\beta \approx 2$ characterizes the costs. Vendor information gives $\$_H \approx \$4000$ for category I furnaces and $40 000 for category II.

VII. Furnace Failure Modes

(1) Creep

Creep is dominant for the metallics, such as the refractory metals and nickel(chromium). It also appears to be important for SiC and $MoSi_2$. For vertical elements having length l supported at one end, failure occurs when the extension exceeds a critical value, δ^*, that causes shortcircuiting. The relevant creep information is summarized in mechanism maps (Fig. 9). The uniaxial strain rate, $\dot{\gamma}$, for loads in the power-law creep domain is[10–13]

$$\dot{\gamma} = \dot{\gamma}_0 \exp\left[\frac{Q_C}{k}\left(\frac{1}{T_M} - \frac{1}{T}\right)\right]\left(\frac{\bar{\sigma}}{\bar{\sigma}_0}\right)^{\bar{n}} \tag{23}$$

where $\bar{\sigma}$ is the stress, $\bar{\sigma}_0$ the reference stress (1 MPa), and T_M the melting temperature. The reference strain rate, $\dot{\gamma}_0$, expressed in this format is material insensitive and is $\sim 3 \times 10^{-6}$/s.[12] The activation energy for the refractory metals is that for coupled lattice and core diffusion. It is of order 500 kJ/mol for tungsten and 350 kJ/mol for molybdenum.[12] The stress exponent is $\bar{n} \approx 5$.

For the nonmetallics, diffusional mechanisms appear to be more important, such that the stress exponent is either 1 or 2. The activation energies are 600 and 450 kJ/mol for SiC and $MoSi_2$, respectively.[14,15]

The life, t_L, obtained from Eq. (23) can be written precisely as given in Eq. (5) with

$$Q_F = Q_c$$

$$T_R = T_M$$

$$t_R = \frac{\delta^*}{l\dot{\gamma}_0}\left(\frac{\bar{\sigma}_0}{\bar{\sigma}}\right)^n \tag{24}$$

(2) Oxidation

Oxidation and fracture are potential failure modes with nonoxide ceramic constituents: SiC and $MoSi_2$. Typically, the oxide surface layer is subject to cracking upon thermal cycling.

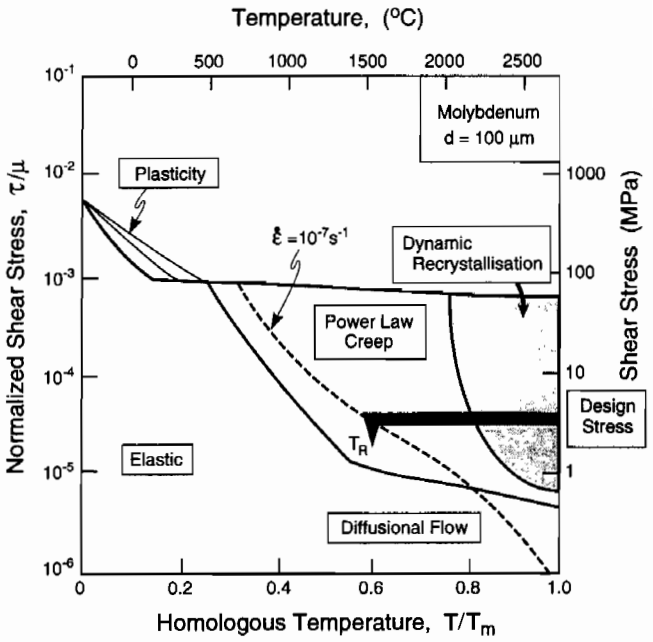

Fig. 9. Deformation mechanism map for molybdenum with 100 μm grain size, emphasizing the regions of power-law creep and dynamic recrystallization.[12] Maximum temperature that avoids excessive creep is ~1600°C for design stresses of order 1 MPa.

These cracks can act as flaws that cause fracture. Because oxide growth is diffusion controlled, the rates can be characterized by a parabolic rate constant, B_O, and an activation energy, Q_O.[16,17] Both depend on the purity of the material, through the composition of the silicate layer. For SiC, B_O and Q_O are 2×10^{-10} m²/s and 220 kJ/mol, respectively, whereas, for $MoSi_2$, the corresponding quantities are 8×10^{-14} m²/s and 130 kJ/mol.

The lifetime is derived by allowing the oxide layer thickness to equal the critical flaw size. The result is

$$t_L = \left(\frac{K_c}{\sqrt{\pi\bar{\sigma}}}\right)^4 \frac{1}{2B_O} \exp\left(\frac{Q_O}{kT}\right) \tag{25}$$

where K_c is the fracture toughness, ~2–4 MPa·m$^{1/2}$ for both materials.

(3) Graphite Furnaces

When graphite furnace constituents are used, they require special considerations. They do not creep significantly below ~2500°C and also are resistant to fracture because of their relatively high toughness and low density. Usually, failure occurs by Joule heating after a sufficient reduction in section, through oxidation. Life thus is limited primarily by the oxygen partial pressure, rather than temperature. The life of graphite furnaces is taken to be $\sim 10^4$ h to include them in these cost simulations.

VIII. Property Development

(1) Functional Forms

Basic information about the phenomena that control property evolution is essential to understand yields and the associated costs. Mechanistic knowledge is preferred, but phenomenological information can suffice. The phenomenology indicates that a property X develops within a time-dependent temperature environment,[18–20] such that an increment in the property function $F(X)$ is related to an increment in time, according to $dF = t_0^{-1} \exp(-Q_p/kT)\, dt$, where t_0 is the time constant in Eq. (4*a*). Thus,

$$F(X) = t_0^{-1} \int_0^t \exp\left(\frac{-Q_p}{kT}\right) dt \tag{26a}$$

The normalization introduced in Eq. (4*b*) is obtained by setting

$$t_Q = t_0 F(X_Q)\ \exp\left(\frac{Q_p}{kT_Q}\right) \tag{26b}$$

With this normalization, Eq. (26*a*) becomes

$$F(X) = F(X_Q) t_Q^{-1} \int_0^t \exp\left[\frac{Q_p}{k}\left(\frac{1}{T_Q} - \frac{1}{T}\right)\right] dt \tag{26c}$$

As elaborated below, $F(X)$ is given with adequate precision by

$$F(X) = \ln \frac{1 - X_0}{1 - X} \tag{27}$$

Here, X_0 is the property magnitude upon entering the high-temperature manufacturing step. Other functional forms can be used, but the implications for the yields are similar.

(2) *Mechanisms*

There are two basic domains of property development: reaction controlled and diffusion controlled. Both domains are thermally activated, with associated activation energies. Prototypical phenomena illustrate the dynamics.

Thermal conductivity development in AlN exemplifies diffusion control.[21–23] It involves the kinetic removal of oxygen dissolved in the grains. It is achieved in the solid state by doping with yttrium aluminates (YAP and YAM), located at grain junctions, which act as host sites for Al_2O_3. It is controlled by diffusion of the oxygen–aluminum defect in AlN. A solution to the diffusion flux gives an expression for the average concentration of oxygen, $c(t)$, as[21]

$$-\ln \frac{c}{c_O} = \frac{\pi^2 D_O}{d^2} \int_0^t \exp\left(\frac{-Q_p}{kT}\right) dt \tag{28}$$

where c_O is the initial concentration, d the grain size, and D_O the diffusion coefficient. The activation energy is $Q_p \approx 350$ kJ/mol. The thermal conductivity, κ_A, is related to the oxygen content by[22]

$$X \equiv \frac{\kappa_A}{\kappa^*} = \left(1 + \frac{c}{c^*}\right)^{-1} \tag{29}$$

where κ^* is the intrinsic thermal conductivity of AlN (300 W/(m·K)) and c^* a reference concentration (1.22 at.%). Combining these results, subject to the assumption that the grain size does not change, gives

$$\ln \frac{X(1 - X_0)}{X_0(1 - X)} = t_0^{-1} \int_0^t \exp\left(\frac{-Q_p}{kT}\right) dt \tag{30}$$

where

$$t_0 = \frac{d^2}{\pi^2 D_O}$$

Some simulation results are plotted on Fig. 10. Although the X dependence of F differs from Eq. (27), the differences are small and the conclusions about yields reached in the next section are unchanged.

Reaction control is exemplified by binder removal from nonoxide green bodies.[24,25] This process must be performed at a low oxygen partial pressure to avert deleterious oxidation. The rate-controlling step is the removal of the carbon subsequent to pyrolysis. This is achieved by vaporization of oxygen from a solid-state source, introduced into the powder. The kinetics typically are controlled by reaction between the carbon and the oxygen, subject to an oxygen pressure dictated by other factors. A result is presented for AlN in a nitrogen environment, with Al_2O_3 as the oxygen source. Here, X depends on the carbon level and approaches unity as the carbon concentration becomes zero. The oxygen partial pressure is related to that for the nitrogen in equilibrium with AlN and Al_2O_3 by

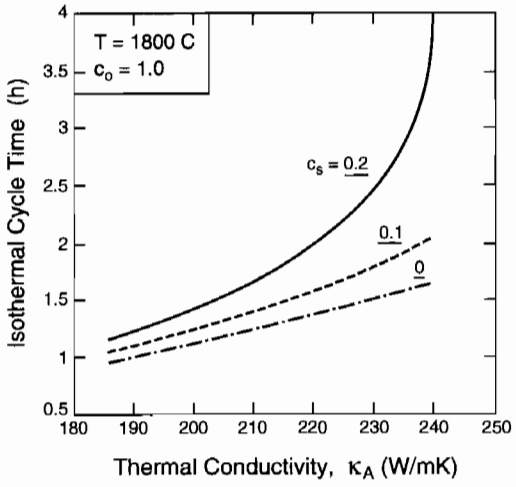

Fig. 10. Effects of isothermal cycle time on the thermal conductivity of AlN.

$$p_{O_2} = p_{N_2}^{2/3}\ \exp\left(\frac{-Q_p}{kT}\right) \tag{31}$$

such that the rate of removal of carbon satisfies[24]

$$(1 - X)^{-1} \frac{dX}{dt} = k^* p_{O_2} \tag{32}$$

where k^* is the rate constant for the reaction. The resulting removal function relating the property X to the temperature history is

$$\ln \frac{1 - X_0}{1 - X} = t_0^{-1} \int_0^t \exp\left(\frac{-Q_p}{kT}\right) dt \tag{33}$$

where

$$t_0 = \frac{1}{k^* P_{N_2}^{2/3}}$$

The activation energy is $Q_p \approx 390$ kJ/mol. Now, $F(X)$ is identical to that in Eq. (27).

IX. Yields

Thermal transients often are dominant in batch processes. The central issue is the different thermal history experienced by components at different locations in the hot zone. These differences cause a spread in the properties/performance of the product, with consequences for the yield. An understanding of these features is central to furnace design and cost minimization. The governing issue is the effect on the yield of the radial variation in properties caused by the temperature gradients. The size of the furnace is dictated by the temperature differences between its center and perimeter. The additional variations in yield associated with material heterogeneity, contained in X_0 and t_0 in Eqs. (26) and (27), are independent of the position in the furnace.

If most devices are to function in accordance with their design, the property X of the product must reside within a range, ΔX_{max}, subject to a minimum value, X_{min}, The properties of those products at the hot zone center, X_c, are systematically lower than those at the outside, X_m, because they experience lower temperatures. The requirements, therefore, are that

$$X_c \geq X_{min} \tag{34}$$

and

$$X_m \leq X_{max} \equiv X_{min} + \Delta X_{max} \tag{35}$$

When both of these inequalities are satisfied, the yield associated with the high-temperature manufacturing step is assumed to be high, i.e., $Y \approx 1$. When Eq. (34) is combined with Eq. (26*c*), the first condition is satisfied at the firing time t_s when

$$t_Q^{-1}\int_0^{t_s} \exp\left[\frac{Q_p}{k}\left(\frac{1}{T_Q}-\frac{1}{T_c}\right)\right] dt \geq \frac{F(X_{min})}{F(X_Q)} \tag{36}$$

where T_c is the temperature at the center of the furnace. The second specification dictates

$$t_Q^{-1}\int_0^{t_s} \exp\left[\frac{Q_p}{k}\left(\frac{1}{T_Q}-\frac{1}{T_m}\right)\right] dt \leq \frac{F(X_{max})}{F(X_Q)} \tag{37}$$

where T_m is the temperature at the outer perimeter of the hot zone. Temperatures in regions in the hot zone lying between the center and perimeter fall between T_c and T_m. Consequently, satisfaction of Eqs. (36) and (37) ensures that property values for the product throughout the furnace are between X_{min} and X_{max}.

The heat-up strategy for simultaneous satisfaction of the inequalities in Eqs. (36) and (37) depends on the size of the furnace. In all cases, the shortest time, t_s, to attain these objectives brings F at the center of the furnace to $F(X_{min})$. Except for small furnaces, t_s also is associated with F attaining $F(X_{max})$ for components at the outer edge of the hot zone. The equalities in Eqs. (36) and (37) are met simultaneously at $t = t_s$. T_* is the goal temperature in the sense that the temperature at the outer perimeter of the hot zone can be increased to T_*, but not higher. When the analysis is performed (Panel C), the power input to the heating elements is adjusted such that the temperature at the outer edge of the hot zone, T_m (effectively the muffle temperature), is increased at a constant rate until T_* is attained and then held constant. The ramp-up time to attain T_* is denoted by t_h.

The specifics of the ramp-up strategy depend on the furnace radius, R. For furnaces satisfying $R \leq R_*$, T_m should be brought up to T_* with no delay ($t_h \approx 0$). The transition radius R_* is specified below. The temperature history at the center of the furnace lags that at the perimeter to a sufficiently small extent such that the inequality at the perimeter is met automatically when that at the center is attained. The furnace size $R = R_*$ is the largest for which T_m can be brought immediately up to the goal temperature. For this furnace, $F = F(X_{max})$ at the perimeter and $F = F(X_{min})$ at the center when $t = t_s$. The ramp-up time, t_h, for furnaces with radii larger than R_* must be chosen to achieve X_{max} at the perimeter of the hot zone simultaneously with X_{min} at its center. This strategy gives the shortest total firing time, t_s. T_m is ramped up to T_* in time t_h and is then held until the property goals are reached for furnaces having radii not too much larger than R_*. Large furnaces never reach T_*. The ramp-up must be conducted very slowly so as to reach the property goals throughout the furnace. The property goals are achieved when the temperature at the outer perimeter, T_m, has not yet reached T_*.

Numerical calculations of the influence of furnace radius, R, on the firing time, t_s (Fig. 11), show that t_s increases sharply for radii above the transition size, R_*. Conversely, small furnaces provide no advantage with respect to the property goals and, moreover, require essentially the same firing time. Thus, R_* represents a useful estimate for the largest radius of an efficient furnace. The firing time for this furnace is readily evaluated, given that T_m is at T_* during the entire history and that $F = F(X_{max})$ is attained at the perimeter when $t = t_s$. Thus, by Eq. (37), the firing time t_s^* associated with the furnace of radius R_* is

$$t_s^* = t_Q \frac{F(X_{max})}{F(X_Q)} \exp\left[\frac{Q_p}{k}\left(\frac{1}{T_*}-\frac{1}{T_Q}\right)\right] \tag{38}$$

The analysis leading to R_* is given in Panel C, with the result

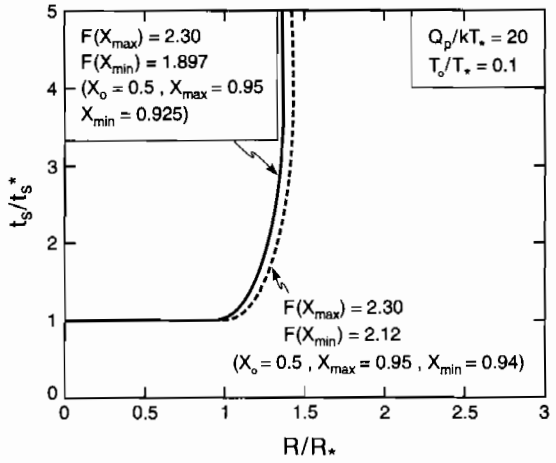

Fig. 11. Effect of hot zone radius, R, on the cycle time, t_s, for two choices of the property goals, for a process with $Q_p/kT_* = 20$.

$$R_* = \left(\frac{F(X_{max}) - F(X_{min})}{AF(X_{max})} a t_s^*\right)^{1/2}$$
$$= \left\{\frac{[F(X_{max}) - F(X_{min})] a t_Q}{AF(X_Q)}\right\}^{1/2} \exp\left[\frac{Q_p}{2k}\left(\frac{1}{T_*}-\frac{1}{T_Q}\right)\right] \tag{39}$$

where A is a weak function of T_* of order unity (Fig. C2). The smaller the permissible spread in the property $\Delta X_{max} = X_{max} - X_{min}$, the smaller must be the furnace. For small ΔX_{max}, $F(X_{max}) - F(X_{min}) \equiv (1 - X_{max})^{-1}\Delta X_{max}$. Equation (39) also emphasizes the connection between the firing temperature, T_*, and the most efficient furnace size. The higher the firing temperature, the smaller the furnace.

The implications of these results are as follows. When the hot zone radius $R \leq R_*$ and the firing time equals t_s^*, the products everywhere in the hot zone satisfy the property specifications. The yield thus would be unity whenever the material entering this process step is homogeneous. Variability in the incoming material would cause $Y \lesssim 1$, randomly throughout the hot zone, independent of the thermal cycle. Satisfaction of these two conditions thus becomes a recipe for achieving consistent, high, yields, essential to a robust manufacturing process. Consequently, imposing these inequalities in the cost formulation allows Y to be fixed at about unity.

Further implications are gained from the scaling results presented in Section IV. Namely, for low costs, the cycle time should be small and the hot zone as large as possible. The consequence is that t_s should be equated to t_s^* and R to R_* to realize the lowest cost. Smaller furnaces also whould give acceptable yields, but the costs would be greater.

X. Cost Simulations

(1) Procedure

A MATLAB program has been developed that embodies the cost formula and the full parameter set described above. This is used to perform cost simulations for various process scenarios. It is facilitated by reexpressing the above results, through the TCF, as terms that depend on the furnace category and its size relative to the maximum ($R \lesssim R_*$), with $t_s \equiv t_s^*$. The procedure for using the program is as follows.

(i) The furnace category (I, II, or III) can be chosen in a preliminary way, starting with knowledge of the vapor-phase requirements and the isothermal kinetics of property evolution.

(ii) The maximum furnace size, R_*, is estimated as a function of T_* from Eq. (39) for X_{max} and ΔX_{max} appropriate to the

product specification (Eq. (27)), with the premise that the kinetics have been calibrated, such that Q_p and T_Q are known.

(iii) The minimum cycle time is determined from Eq. (38) as a function of T_* with an initial choice made for the hot zone diffusivity, preferably based on a calibration, but otherwise estimated from Panel A. This allows the annual production to be assessed from Eq. (6), for a reasonable estimate of the time t_{st} needed to cool and stack the parts into the furnace. If this production is greater than the expected market volume, there are two options: either the furnace could be operated below capacity or a smaller furnace could be substituted. Both options cause a penalty on cost per part that can be calculated in the manner described below. Conversely, when the market expectations are larger, the furnace size would be set at R_* and a longer furnace used or multiple furnaces used. This situation is considered in the next section.

(iv) The failure mechanism for the furnace elements is selected, using for guidance the information presented in Section VII. This defines Q_F, T_F, and T_R for each of the furnace options.

(v) The cost per part is calculated as a function of the goal temperature, T_*. This is done for a range of a, ΔX_{max}, and X_{max} around the magnitudes believed to be relevant to the product and the furnace. The temperature ratio between the heating elements and the muffle is used, if known. Otherwise, the estimate presented in Panel A is assumed. This factor can have an important influence on the element life.

(2) *Furnace Capacity*

The optimum furnace size (Eq. (39)) for a given scenario has an implied annual production obtained by inserting $R = R_*$ and $t_s = t_s^*$ into Eq. (12*d*). The result is

$$\zeta = \frac{Lfat_Y[F_{max}(X_{max}) - F_{min}(X_{min})]t_L}{V_p A F_{max}(X_{max})\{N_L[(1+\alpha)t_s + t_{st}] + t_r\}} \tag{40}$$

That is, the annual production is essentially independent of the cycle time and, consequently, of the goal temperature, until T_* is high enough to cause frequent furnace failure. The most important determinants of ζ for parts of fixed size, V_p, are the specification range, ΔX_{max}, and the thermal diffusivity of the hot zone. This is apparent in the following simulations.

The production level has important cost consequences. At this production, the cost per part has its minimum value, $\Delta\$_{min}$, as elaborated in the following illustration. However, when the market demand is smaller than this production, there is an increase in the cost per part, because the throughput is smaller than the capacity of the furnace. The effect can be determined by reducing the number of downtimes through a capacity coefficient, η, such that N_{DOWN} in Eq. (12*b*) is replaced by

$$N^*_{DOWN} = \frac{\eta t_D}{N_L[t_s(1+\alpha) + t_{st}] + t_r} \tag{41}$$

where η ranges between unity at full capacity and zero whenever the furnaces are idle. The effect of annual sales on the cost per part can be determined by incorporating η into the simulation, as illustrated below.

When the annual production at the optimum furnace size is lower than the market volume, more than one furnace is needed to satisfy demand. Then, the acquisition of additional furnaces causes the cost to increase again whenever one of the extra furnaces is operating below capacity. At this stage, nontechnical factors, such as discounts on furnace acquisitions, become important, but beyond the scope of the TCF.

(3) *Illustration*

The information generated by the simulation program is illustrated by using parameters relevant to a high-temperature process, such as thermal conductivity development in sintered AlN products.[21,23] The parameters to be used are summarized on Table II. Other choices for the times t_r and t_{st} can be made, but they have little effect on the overall cost trends, illustrated on Figs. 12–17, as discussed below.

Table II. Parameters Used for Cost Simulations Illustrated in Section X

Parameter	Value
Activation energy, Q_p (kJ/mol)	390
Process reference temperature, T_Q (°C)	1900
Furnace stacking fraction, f	0.3
Furnace thermal diffusivity, a (m/s)	10^{-6}–10^{-5}
Stacking time, t_{st} (h)	2
Heating element replacement time, t_r (h)	48
Relative heating element temperature, T_h/T_m	1.1
Depreciation time, t_D (years)	5
Utility cost, ϕ_u (dollars/(kW·h))	0.1

There is a temperature T_{min} below T_Q at which the manufacturing cost is a minimum, $\Delta\$_{min}$ (Fig. 12). This trend results because of the competing influences of a shorter cycle time and a decreased element life at higher temperature. The effect is primarily a consequence of the reduced throughput that occurs when the failed furnace parts need to be replaced, rather than the cost of the replacement parts per se. The importance of furnace failures is exacerbated upon including labor costs, as explored below. The cost at T_{min} is hereafter used as the metric for assessing trends with the other variables. A subroutine has been written into the MATLAB program to enable this minimum to be determined.

Results obtained for three different furnaces are plotted on Figs. 13–15. Because X_{max} is prescribed and ΔX_{max} allowed to vary, then, for a particular furnace choice, the goal temperature at the cost minimum, T^*_{min}, as well as the corresponding cycle time, t_s^{min}, are essentially independent of both the hot zone thermal diffusivity, a, and the property specification range, ΔX_{max}. The ranges found for the three furnace categories are summarized on Table III. The contribution to $\Delta\$$ from power usage, $\$_1$, is negligibly small in all of the simulations, even though the utility cost (Table II) is taken to be quite high.

For each furnace, T^*_{min} is ~ 200°–250°C lower than the rating temperature, T_R (see Tables I and II). This is consistent with intuition and reflects the effect of the temperature difference $T_R - T^*_{min}$ on the failure rates of the furnace constituents. That is, when this temperature difference is small, the furnace failure rate is high, causing the throughput to be severely diminished. Conversely, at large temperature differences, the cycle time becomes long, again diminishing the throughput. These competing effects lead to an optimum T^*_{min} and minimum cost.

The cycle times are a direct consequence of the optimum T^*_{min}. Namely, the higher T^*_{min}, the lower t_s^{min} because of the exponential effect of temperature. Moreover, for a fixed property maximum, t_s^{min} is insensitive to ΔX_{max} and a at the optimum furnace size, R_*. This happens because X_{max} is controlled by the temperature history at the outer region of the hot zone, and the furnace radius adjusts (see Fig. 14) such that X_{min} at the center is realized when X reaches X_{max} at the outside. Further studies are needed to assess the effect of the process, Q_p, and the replacement time, t_r, on T^*_{min}.

The trends at the cost minimum associated with the above goal temperature and cycle time trends are as follows.

(i) The major consequence is the convolution of the throughput with furnace acquisition and replacement costs, reflected in the effect of furnace category on $\Delta\$_{min}$. That is, although the molybdenum furnaces are less costly than tungsten furnaces, the much longer cycle time of the former causes the cost per part to be much higher (Figs. 13(a) and (b)). Consequently, tungsten is the preferred construction material on a cost per part basis for category II furnaces. However, $\Delta\$_{min}$ remains lower for the $MoSi_2$ category I furnace (Fig. 13(c)), even though the cycle time is longer. This cost reduction reflects the lower furnace acquisition and replacement cost. This furnace thus is preferred, provided that the gas-phase composition requirements (particularly the oxygen partial pressure)

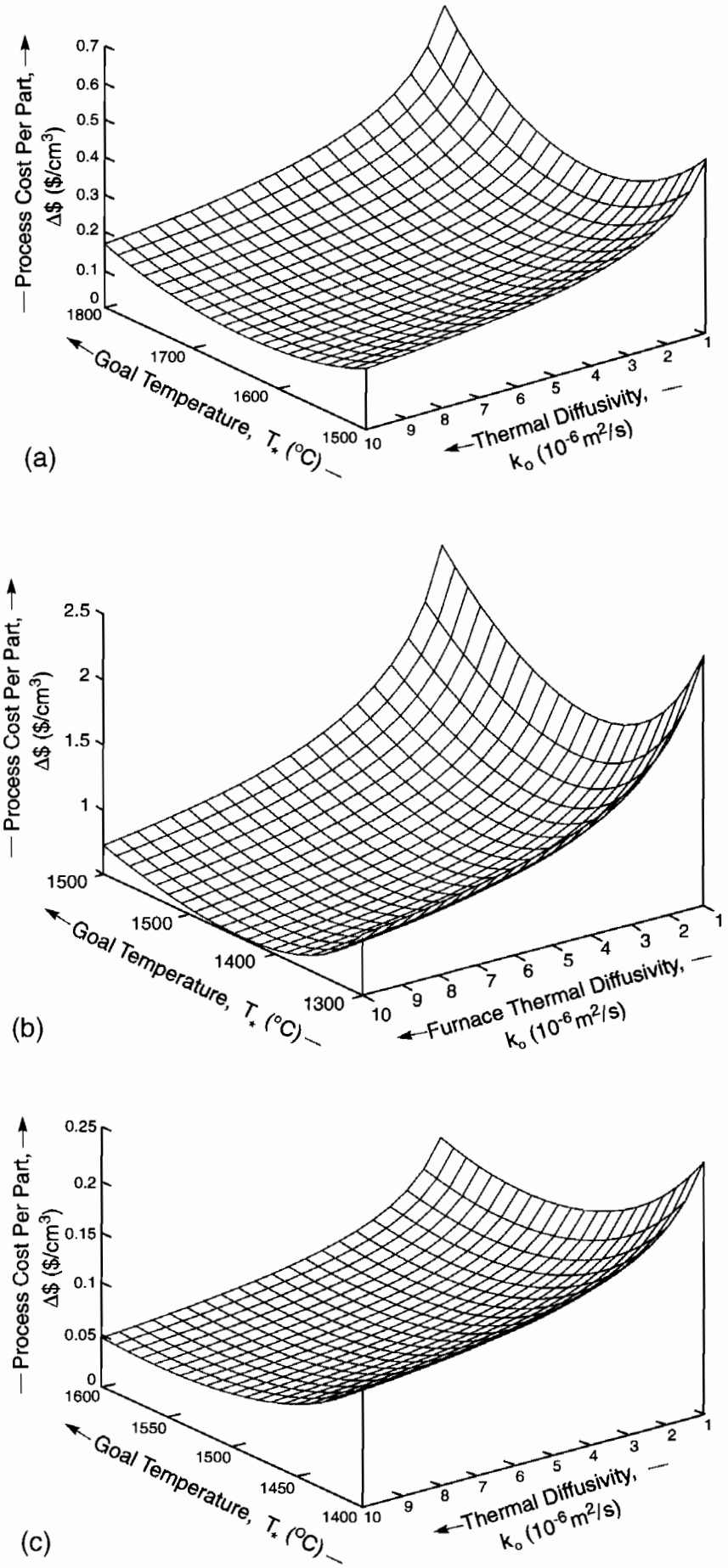

Fig. 12. Combined effects of hot zone thermal diffusivity and goal temperature on the manufacturing cost of cm^3 parts determined for a process characterized by Table II: (a) tungsten, (b) molybdenum, and (c) $MoSi_2$ (T_Q = 1900°C).

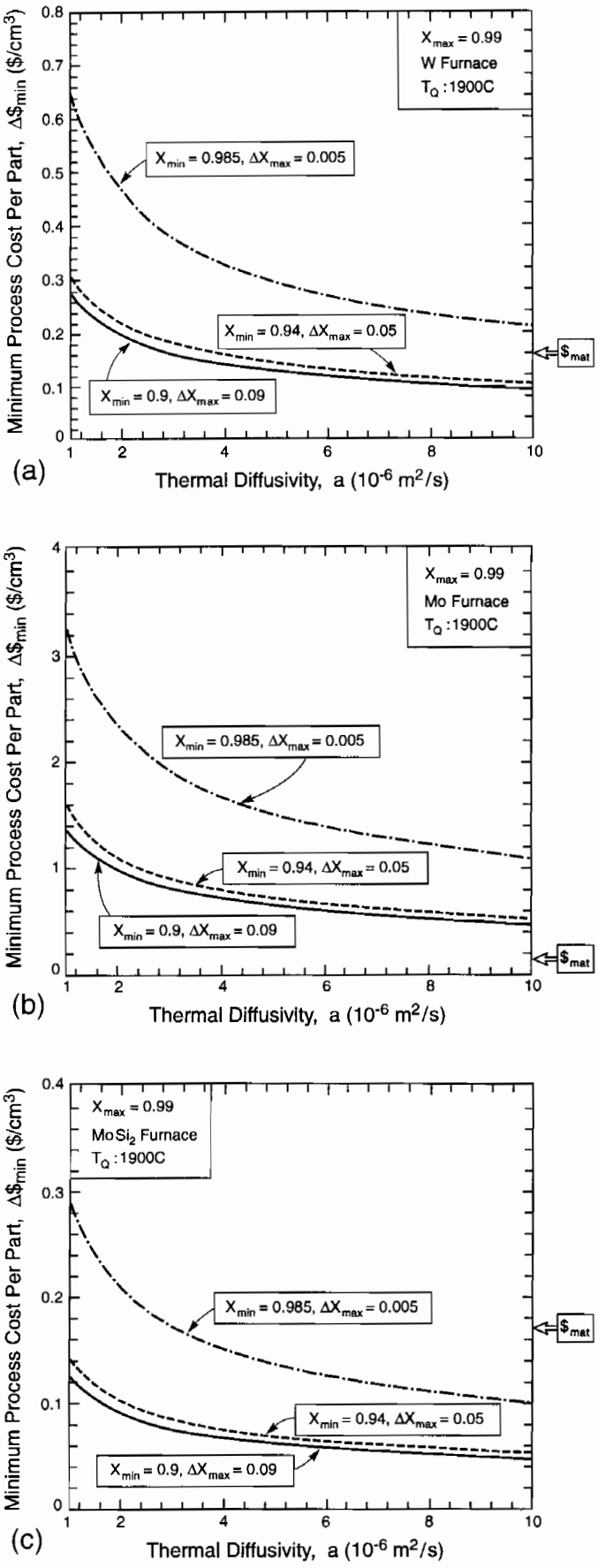

Fig. 13. Variation in the manufacturing cost minimum for the process characterized by Table II, with $T_Q = 1900°C$, as a function of the hot zone thermal diffusivity, for several values of the property specification range ΔX_{max} with $X_{max} = 0.9$: (a) tungsten, (b) molybdenum, and (c) $MoSi_2$.

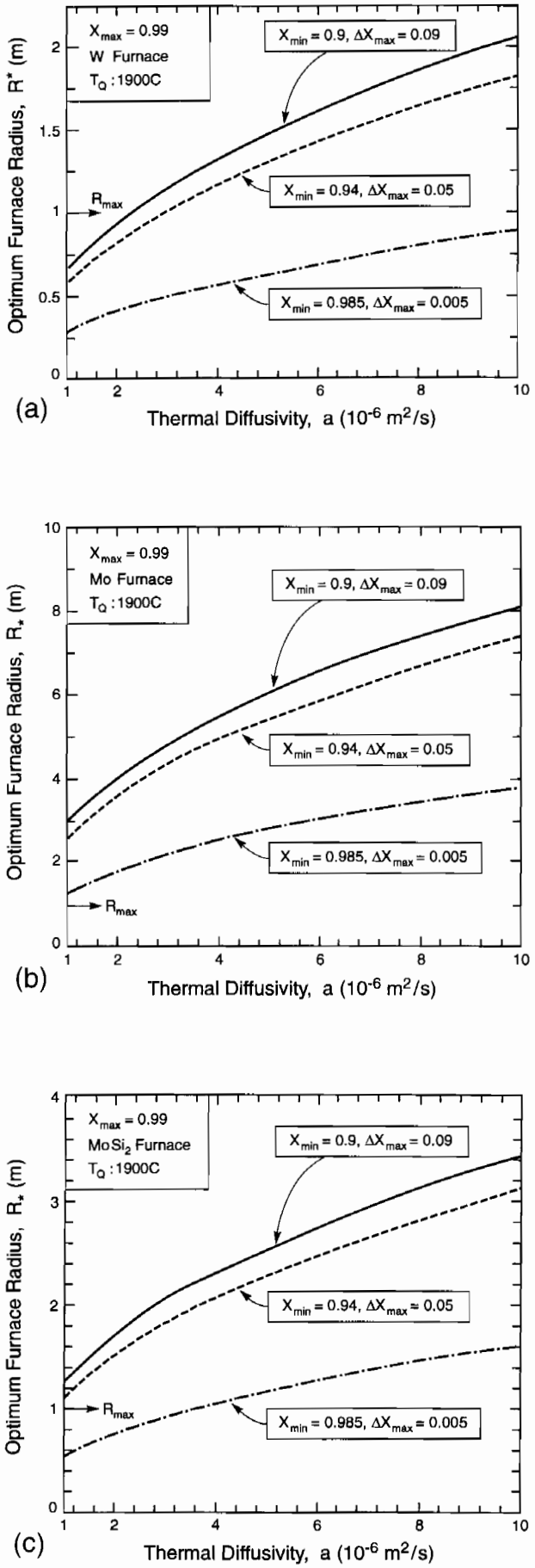

Fig. 14. Variation in the optimum furnace radius, R_*, with the hot zone thermal diffusivity for several ΔX_{max} with $X_{max} = 0.9$: (a) tungsten, (b) molybdenum, and (c) $MoSi_2$.

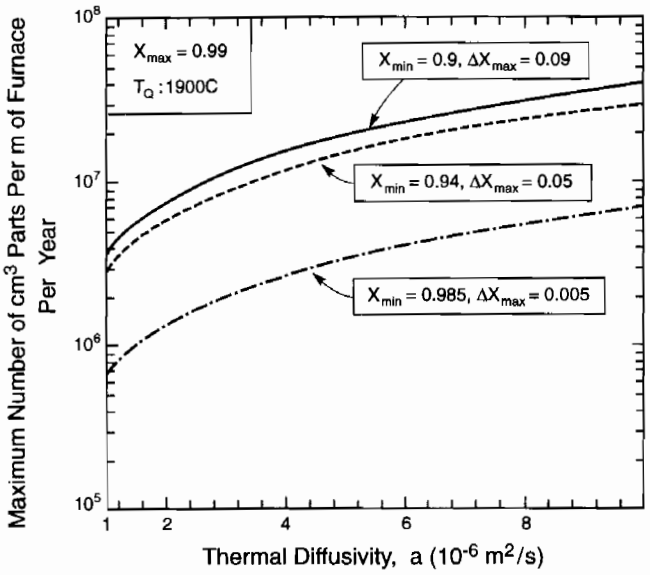

Fig. 15. Maximum annual production of cm^3 parts per meter of furnace at the cost minimum.

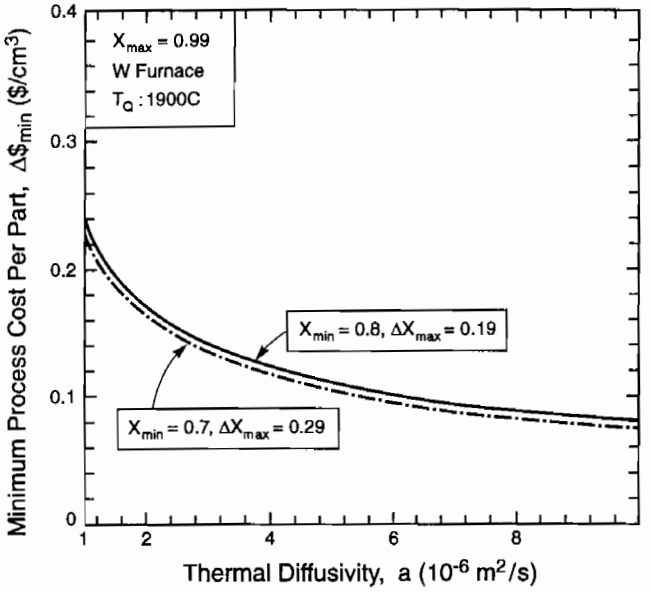

Fig. 16. Effect on cost of relaxing the constraint on the property range ΔX_{max} for a tungsten furnace.

Table III. Conditions at Cost Minimum for Process Characterized by Table II

Furnace	Goal temperature range, T_* (°C)	Cycle time range t_s (h)
Tungsten	1630–1640	145–160
Molybdenum	1420–1440	2500–3200
$MoSi_2$	1530–1560	400–600

can be attained with the use of a muffle tube. Otherwise, a tungsten, category II, furnace is preferred.

(ii) The cost minimum (Fig. 13) systematically decreases as the thermal diffusivity of the hot zone increases, particularly at small a. Consequently, there is an incentive to design the furnace hot zone to achieve high diffusivity. For reference purposes, the material cost (at \$20/lb) is indicated on Fig. 13 to reveal that the manufacturing costs can be lower than material costs, particularly when a high-thermal-diffusivity furnace is used and the product specification range is not too narrow.

(iii) When the furnace size and the goal temperature have been optimized, the cost is quite insensitive to the property range, ΔX_{max}, whenever it exceeds ~0.05 (Fig. 13). Consequently, there is no cost benefit by further relaxing the specification range (Fig. 16). Conversely, when high tolerance is required ($\Delta X_{max} = 0.005$), the costs increase dramatically. This effect provides the critical link between performance and manufacturing. Further studies will elaborate on this linkage.

The costs expressed on Figs. 12 and 13 have implied values of furnace radius and annual production. These are indicated on Figs. 14 and 15. The furnace radii at the cost minimum require some discussion. These radii become quite large as the property range, ΔX_{max}, becomes large (Fig. 14), especially for those furnaces that require smaller T^*_{min} (molybdenum and $MoSi_2$). In practice, furnaces with R_* exceeding ~1 m cannot be constructed within the cost framework represented by Eq. (8), resulting in an effective size maximum, R_{max}. Consequently, as a practical expedient for cost computation, whenever $R_* > R_{max}$, the furnace size should be set at R_{max} and the cost recomputed.

The annual production (Fig. 16) also is significant, because market volumes either larger or smaller result in higher costs (Eq. (40)). The effect of reduced capacity is plotted on Fig. 17, as the trend in Δ\$ with the annual production, as a fraction η, of capacity being used. Market volume thus is an important factor affecting manufacturing cost.

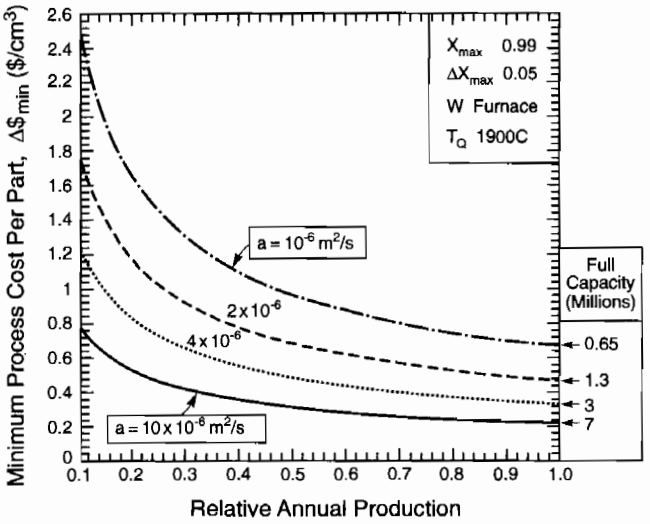

Fig. 17. Effect of furnace capacity factor η on the manufacturing cost per part, with the associated annual production indicated.

An important approach for reducing cost entails increases in the property development rate, X, whereupon the same property levels, X, develop in time t_Q at *lower* T_Q. The explicit benefits that derive from decreasing T_Q to 1600°C (from 1900°C) are illustrated on Fig. 18. There is almost an order of magnitude reduction in $\Delta\$_{min}$ for either tungsten or $MoSi_2$ furnaces, with manufacturing costs as low as \$0.01/cm^3 for the latter. Such low costs are obtained when a high-thermal-diffusivity furnace is used, and when the specification range is not overly stringent ($\Delta X_{max} \geq 0.05$). For the AlN process, a reduction in T_Q can, in principle, be achieved by decreasing the grain size as well as decreasing the initial oxygen concentration. Further studies exploring these costs benefits are in progress.

(4) Other Factors

Labor costs are not included in the present version of the TCF. They are clearly important and can be added into the code in a straightforward manner once the labor requirements have been specified. For example, the unloading and reloading of the furnaces as well as the replacement of failed furnace constituents require labor. The former contributes to the cost per part as

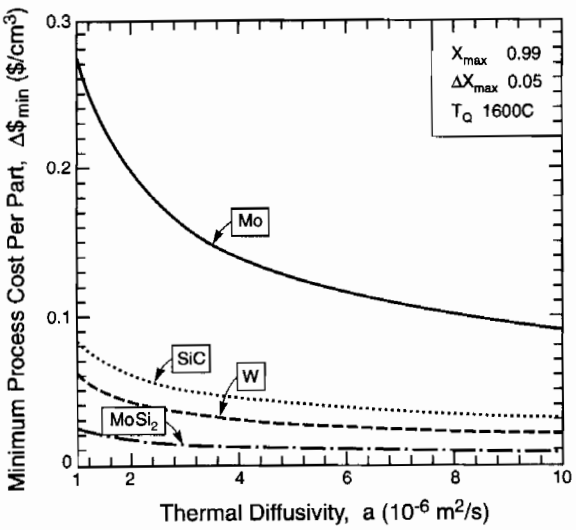

Fig. 18. Minimum costs per part for four furnaces when T_Q = 1600°C. Comparison with Fig. 13 indicates the cost reduction upon decreasing T_Q from 1900°C.

$$\$_{lab} = \frac{t_{st}\phi_L}{fR_*^2 L(1+\alpha)t_s} \tag{42}$$

$\$_{lab}$ can be determined from R_*, given by Fig. 14, and t_{sg} given by Table III. However, other circumstances, which are beyond the scope of the TCF assessment, affect the overall use of labor.

Another potentially important issue is the occurrence of a deleterious mechanism within the material that limits the operating temperature to T_{max}. When T_{max} is above that at which the cost minimum, T_{min}, occurs, all of the preceeding results continue to apply. However, when $T_{max} < T^*_{min}$, T_{max} becomes a constraint on the cost and dictates the choice of furnace to that giving the lowest cost when $T_* = T_{max}$. Further studies will elaborate this issue.

XI. Summary

A technical cost framework has been used to develop a cost simulation tool for the high-temperature manufacturing of small parts and devices. It provides a visualization of the cost consequences of decisions about product property specifications through their ramifications on furnace size, operating temperature, and thermal diffusivity of the hot zone. The important influence of market volume on cost emerges in a natural manner. The tool has many options for user input but also contains best estimates of parameters that are difficult to access from the open literature: particularly, furnace acquisition cost and heating-element failure coefficients. When these coefficients are known more precisely from independent information, they can replace the present estimates.

It is believed that the simulation tool has practical utility because many interdependencies are not obvious. Simulation facilitates decisions about furnace design (including size and category), about preferred operating temperature, and about corresponding cycle time. Preliminary comparisons can be made between manufacturing and material costs to make projections about markets. Further applications of the technique will be presented in future studies.

References

[1]M. F. Ashby, *Materials Selection in Mechanical Design*; pp. 10–50. Pergamon Press, Oxford, U.K., (1992).

[2]C. G. E. Mangin, J. Neely III, and J. P. Clark, "The Potential for Advanced Ceramics in Automotive Engine Application," *JOM*, **45**, 23 (1993).

[3]J. P. Clark and J. V. Busch, "Materials Markets: Modelling"; pp. 2855–61 in *Encyclopedia of Materials Science and Engineering*. Edited by M. B. Bever. Pergamon Press, Oxford, U.K., 1986.

[4]J. A. Isaacs, F. R. Gield, and J. P. Clark, "Automotive Materials: Competition among Materials for Powertrain Applications"; pp. 191–98 in *Encyclopedia of Advanced Materials*. Edited by D. Bloor *et al.* Pergamon Press, Oxford, U.K., 1994.

[5]T. F. Klimowitz, "The Large-Scale Commercialization of Aluminum-Matrix Composites," *JOM*, **46**, 49 (1991).

[6]J. P. Holman, *Heat Transfer*; pp. 97–99. McGraw-Hill, New York, 1976.

[7]J. D. Poirier and G. M. Geiger, *Transport Phenomena in Materials Processing*; pp. 100–27. TMS Warrendale, PA, 1994.

[8]F. P. Incropera and D. P. DeWitt, *Fundamentals of Heat and Mass Transfer*, 3rd ed.; Chs. 7–9. Wiley, New York, 1990.

[9]H. S. Carslaw and J. C. Jaeger, *Conduction of Heat in Solids*; pp. 29–33. Oxford University Press, Oxford, U.K., 1995.

[10]M. F. Ashby, "A First Report on Sintering Diagrams," *Acta Metall.*, **22**, 275–89 (1974).

[11]R. M. Cannon and R. L. Coble, *Processing of Crystalline Ceramics*; pp. 151–70. Edited by H. Palmour and R. F. Davis. Plenum Press, New York, 1978.

[12]H. Frost and M. F. Ashby, *Deformation Mechanisms Maps*. Pergamon Press, Oxford, U.K., 1982.

[13]A. M. Brown and M. F. Ashby, "Correlations for Diffusion Constants," *Acta Metall.*, **18**, 1085–101 (1980).

[14]P. M. Sargent and M. F. Ashby, "Deformation-Mechanism Maps for Silicon Carbide," *Scr. Metall.*, **17**, 951–57 (1983).

[15]K. Sadaranda, C. R. Feng, H. Jones, and J. Petrovic, "Creep of Molybdenum Disilicide Composites," *Mater. Sci. Eng.*, **A155**, 227–39 (1992).

[16]J. A. Costello and R. E. Tressler, "Oxidation Kinetics of Silicon Carbide Crystals and Ceramics," *J. Am. Ceram. Soc.*, **69**, 674–81 (1986).

[17]J. Schlichting, "Oxygen Transport through Silica Surface Layers on Silicon-Containing Ceramic Materials," *High Temp.-High Pressures*, **14**, 717–24 (1982).

[18]D. R. Wall and H. Y. Cohn, "Removal of Carbonaceous Residue with Wet Hydrogen in Greensheet Processing for Multilayer Ceramic Module: I Residue Formation and Intrinsic Chemical Kinetics," *J. Am. Ceram. Soc.*, **73**, 2944–52 (1990).

[19]J. Bilbao, A. Romero, and J. M. Arandes, "Kinetic Equation for the Regeneration of a Solid Catalyst by Coke-Burning," *Chem. Eng. Sci.*, **38**, 1356–60 (1983).

[20]J. F. Johnstone, C. Y. Chen, and D. S. Scott, "Kinetics of Steam–Carbon Reaction in Porous Graphite Tubes," *Ind. Eng. Chem.*, **44**, 1564–69 (1952).

[21]A. G. Virkar, T. B. Jackson, and R. A. Cutler, "Thermodynamic and Kinetic Effects of Oxygen Removal on the Thermal Conductivity of Aluminum Nitride," *J. Am. Ceram. Soc.*, **72**, 2031–42 (1989).

[22]J. H. Harris and R. A. Youngman, "Light-Induced Defects in Aluminum Nitride Ceramics," *J. Mater. Res.*, **8**, 154–62 (1993).

[23]Y. Kurokawa, K. Utsumi, and H. Takamizawa, "Development and Microstructural Characterization of High-Thermal Conductivity Aluminum Nitride Ceramics," *J. Am. Ceram. Soc.*, **71**, 588–89 (1989).

[24]D. Wall and A. G. Evans, "Mechanisms of Carbon Removal from Non-Oxide Green Bodies in Reducing Environments," *J. Am. Ceram. Soc.*, in review.

[25]P. Lefort and M. Billy, "Mechanisms of AlN Formation through the Carbonthermal Reduction of Al_2O_3 in a Flowing N_2 Atmosphere," *J. Am. Ceram. Soc.*, **76**, 2295–99 (1993).

[26]M. Jakob, *Heat Transfer*; p. 57. Wiley, New York, 1957. □

Professor Anthony Evans was educated at Imperial College, London, U.K. He has worked in the United States since 1971 at various locations, including NIST, Rockwell International, and University of California (Berkeley and Santa Barbara). Professor Evans is now at Harvard University. His research on ceramics and their composites largely has been on mechanical properties. The present article reflects recent interests in manufacturing issues. He is the recipient of several awards from The American Ceramic Society and elsewhere and a member of the National Academy of Engineering.

John W. Hutchinson is Gordon McKay Professor of Applied Mechanics in the Division of Engineering and Applied Sciences at Harvard University. He obtained his bachelors degree in engineering mechanics at Lehigh University and his Ph.D. in mechanical engineering at Harvard University. His technical interests fall within the general areas of engineering materials and structures, and specifically within the subjects of plasticity, fracture, and buckling.

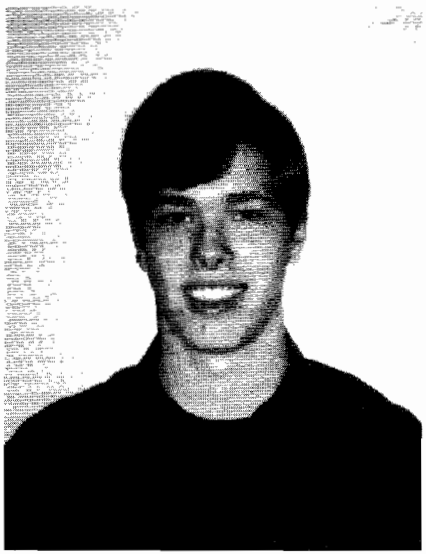

Robert G. Hutchinson is a sophomore at The University of Michigan, where he is concentrating in materials science and engineering. He participated in the project on developing the technical cost model as a member of the REU Program (Research Experience for Undergraduates) organized within the Materials Research Laboratory at Harvard University.

Yuki Sugimura is a postdoctoral researcher in the Division of Engineering and Applied Sciences at Harvard University. She earned her Sc.B., M.S., and Ph.D. degrees in materials science at Brown University in 1989, 1991, and 1994, respectively. She has investigated the development of matrix microstructure and its effect on the overall mechanical properties of metal-matrix composites as well as fatigue crack propagation behavior in composites and materials involving interfaces. Her current research activity involves deformation behavior of metallic foams under monotonic and cyclic loads as well as metal–ceramic interface mechanics.

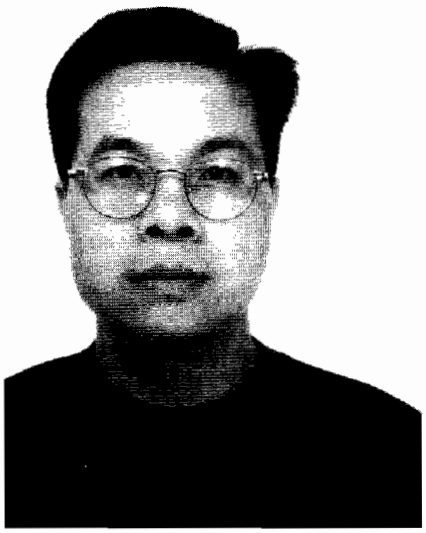

Tian Jian Lu received the B.S. and M.E. degrees in applied mechanics from Xian Jiaotong University, China, in 1984 and 1987, and the M.S. and Ph.D. degrees in engineering sciences from Harvard University in 1993 and 1995, respectively. Since 1996, he has been a university lecturer in Cambridge University Engineering Department. He also is a joint professor in the State Key Laboratory of Materials Strength and Structural Vibrations (MSSV) at Xian Jiaotong University, China. Dr. Lu's research interests include reliability analysis of structural components, heat transfer and sound absorption in cellular metal systems, constitutive laws of porous materials, thermal shock resistance of solids, micromechanics of fiber-reinforced ceramic-matrix composites, fatigue crack initiation and propagation in metals, and thermal management of high-power electronic devices. He has published more than 50 technical articles in professional journals. He has consulted for industry on problems in fracture mechanics, finite-element modeling, heat transfer, and heat-sink design.